Graphical Abstract

Click here to download high resolution image

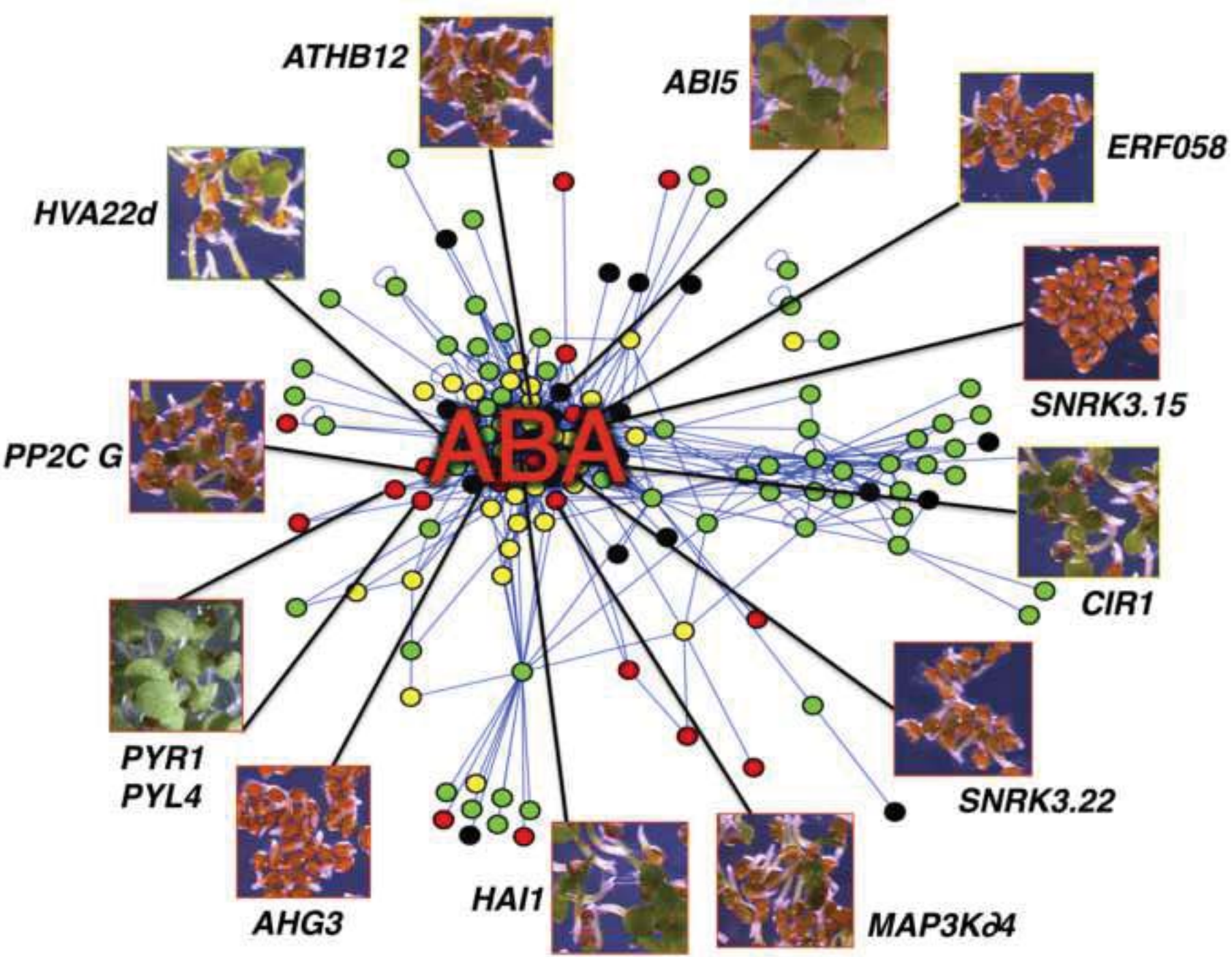

Highlights

- High quality ABA network encompassing 500 interactions among 138 proteins
- Doubled the number of proteins that interact with core ABA signaling components
- Identified a new SNRK3 signaling module that attenuates early ABA responses
- Mapping co-expression predicted the function of genes under abiotic stresses

A meso-scale abscisic acid hormone interactome reveals a dynamic signaling landscape in Arabidopsis

Shelley Lumba[1], Shigeo Toh[1], Louis-François Handfield[2], Michael Swan[1], Raymond Liu[1], Ji-Young Youn[3], Sean R Cutler[4], Rajagopal Subramaniam[5], Nicholas Provart[1], Alan Moses[1,2], Darrell Desveaux[1,6] & Peter McCourt[1,6]

[1] Cell & Systems Biology, University of Toronto and the Centre for The Analysis of Genome Evolution and Function, University of Toronto, Toronto, Ontario, M5S 3B2, Canada.

[2] Department of Computer Science, University of Toronto, Toronto, Ontario, M5S 2E4, Canada.

[3] Banting and Best Department of Medical Research, Terrence Donnelly Centre for Cellular and Biomolecular Research, University of Toronto, Toronto, M5S 3E1, Canada.

[4] Department of Botany and Plant Sciences and the Center for Plant Cell Biology, University of California-Riverside, Riverside, California, USA.

[5] Agriculture and Agrifood Canada, 960 Carling Ave, Ottawa, ON, K1A 06C, Canada.

[6] To whom correspondences should be addressed; darrell.desveaux@utoronto.ca; peter.mccourt@utoronto.ca

Running title: **ABA signaling networks in plants**

The sequiterpenoid abscisic acid (ABA) mediates an assortment of responses across a variety of kingdoms including both higher plants and animals. In plants, where most is known, a linear core ABA signaling pathway has been identified. However, the complexity of ABA-dependent gene expression suggests ABA functions through an intricate network. Here, using systems biology approaches that focused on genes transcriptionally regulated by ABA, we defined an ABA signaling network of over 500 interactions among 138 proteins. This map greatly expanded ABA core signaling but was still manageable for systematic analysis. For example, functional analysis was used to identify an ABA module centered around two SNF-like kinases. We also used co-expression analysis of interacting partners within the network to uncover dynamic sub-network structures in response to different abiotic stresses. This comprehensive ABA resource allows for application of approaches to understanding ABA functions in higher plants.

INTRODUCTION

ABA is a sequiterpenoid based compound that has biological activity in a variety of organisms ranging from sponges and human parasites to mammalian cells in addition to plants (see Wasilewska et al., 2008 and Li et al., 2011 for review). In animals for example, ABA appears to stimulate immune responses and insulin release from pancreatic cells. It has also been implicated in heat and light stress responses in animals. But the absence of a good model genetic system to study ABA in animals makes it difficult to understand the mechanisms underlying the role of ABA in mediating various responses. By contrast, in higher plants and particularly in the model *Arabidopsis thaliana,* functional analysis has shown ABA to be an important hormone in both embryonic and vegetative growth and development. In vegetative tissues, ABA protects plants

from a variety of abiotic stresses such as drought, temperature, salt and oxidative stresses (Nakashima and Yamaguchi-Shinozaki, 2013; Cramer et al., 2011). For this reason, the synthesis and signal transduction of ABA has been intensively studied not only at a fundamental level but also for potential applications in crop based biotechnology (Ben-Ari, 2012; Wilkinson et al., 2012).

In higher plants, ABA appears to regulate both "fast responses" relating to ion channel flux in the guard cell and "slow responses" related to gene expression within the nucleus (see Hubbard et al., 2010 for review). Surprisingly genetic dissection of ABA signaling defines a relatively simple hierarchical signaling pathway that appears to regulate both responses (**Figure 1A**) (Cutler et al., 2010; Hubbard et al., 2010; Lumba et al., 2010). In the case of transcriptional responses, ABA binds to the PYR/PYL/RCAR (PYL) family of receptors, thereby allowing them to interact and inhibit a class of A-type Protein Phosphatase 2Cs (PP2Cs). PP2C inactivation permits a small set of class 3 SNF-1 related protein kinase 2s (SNRK2s) to phosphorylate a collection of basic leucine zipper (bZIP) transcription factors (ABFs). The phosphorylation of ABFs activates downstream gene expression through the cis-acting ABA response element (ABRE). ABA core components also directly regulate S-type anion channels SLAC1 and SLAH3 in the guard cell, demonstrating the core ABA signaling pathway also has cytosolic "fast response" targets (Geiger et al., 2011; Brandt et al., 2012).

While the core signaling pathway illustrates the importance of ABFs in ABRE-dependent gene expression, the transcription factors that regulate the expression of the many other genes induced by ABA but lacking ABREs in their promoters, have not been clearly defined. For example, up to 11 different transcription factor families have been implicated in ABA-related processes (Fujita et al., 2011). Moreover, because of the role of ABA in protecting against

various environmental stresses, the core ABA signaling pathway must work in coordination with signaling pathways involved in drought, heat, salt and cold stress (Hey et al., 2010; Huang et al., 2012). The overlap between primary ABA signaling and stress response pathways results in the formation of sub-networks that could reveal points of crosstalk and potential ways of modulating the ABA signal.

System-based approaches are beginning to be used to link signaling pathways into larger complex networks in plant biology (Van Leene et al., 2011; *Arabidopsis* Interactome Mapping Consortium, 2011; Lalonde et al., 2010). As networks become larger, however, interactions between components can quickly scale to a point where defining the roles of any particular protein is challenging (Hartwell et al., 1999; Spirin and Mirny, 2003). With these considerations, we used specific parameters to expand the components involved in ABA signaling whilst keeping the signaling network space experimentally manageable. We did this by first building a protein-protein interaction (PPI) network or interactome via yeast two-hybrid technologies in which the input gene set was limited to genes involved in the primary transcriptional response to ABA. Because PPIs occur more frequently within a group of co-regulated genes than a randomly expressed gene set, this ABA-regulated gene set should be enriched for interacting protein partners (Ge et al., 2001). In addition, much of the core ABA signaling pathway is transcriptionally regulated by ABA, thus these core components provide a framework on which to expand the signaling network. Next, unlike many yeast-based interactome networks, which use a single reporter system, we generated our ABA network using multiple reporter outputs and then integrated these outputs using machine learning algorithms and imaging software. This analysis allowed us to rank protein interactions based on statistically derived confidence levels.

This multilayered approach generated the "Transcriptionally Regulated ABA Interactome

Network" (TRAIN), which encompassed over 500 additional PPIs of high quality. The TRAIN can be integrated with published protein interaction databases to build an expanded network (eTRAIN) of over 1000 interactions. Our approach verified most of the published ABA-related interactions and expanded core ABA signaling by more than 50 proteins. The development of the TRAIN is a useful resource for plant hormone researchers. For example, because the interaction space is experimentally tractable, systematic and targeted functional analysis can be performed. As a proof of principle, we identified a 20-member sub-network centered around two SNRK3s, which appears to negatively modulate ABA responsiveness. We also show the TRAIN can be used to examine the dynamic structure of protein networks in response to various abiotic stresses. By mapping stress dependent co-expression of gene pairs over multiple time points and tissues, we were able to visualize how the wiring of the TRAIN sub-networks changed in response to specific abiotic stresses. We used this information to discover an important transcription factor involved in Arabidopsis salt stress response.

RESULTS

The Transcriptionally Regulated ABA Interactome Network (TRAIN)

To identify a collection of genes that were rapidly regulated by ABA, we performed whole genome transcript profiling on an Arabidopsis mutant deficient in ABA synthesis (*aba2*) (Léon-Kloosterziel et al., 1996). The use of an auxotroph versus a wild type plant not only avoided complications involving the plant's response to exogenous and endogenous ABA pools but may also sensitize the transcription of both major and minor genes in response to ABA application. Because we were using seedlings deficient in endogenous ABA, we could limit ABA exposure to low concentrations (1 μM) for a short duration (6 hours). In addition, both ABA-treated and

untreated plants were exposed to the translational inhibitor, cycloheximide, to enrich for primary transcriptional events (**Figure S1**). Using these experimental conditions, we identified 282 genes (282set) whose expression changed two-fold or more in response to ABA versus untreated seedlings (**Table S1**). Within the 282set, we found that 85.2% and 60.2% of genes that were induced and repressed by ABA, respectively, are also identified in other ABA transcriptome studies, suggesting the 282set is a good representation of ABA regulated genes (**Table S1**). Moreover, the ABRE promoter element was significantly over-represented (125 of 282 genes, p-value 3.98×10^{-18}) and approximately 80% of the 282set genes were dampened in the *snrk2.2/2.3/2.6* triple mutant, which is defective in core ABA signaling (**Figure 1B**) (Fujita et al., 2009*)*. Interestingly, although the 282set contained many well characterized ABA-responsive genes, approximately 40% of the gene set fell below the two-fold expression cutoff that is often the basis of hormonal-based gene expression experiments, but follow the same trend of induction or repression by ABA, which suggests *aba2-2* did sensitize transcription to ABA treatment (**Table S1**). In summary, the 282set represented a transcriptionally sensitized gene set that is mostly regulated by the core ABA signaling pathway.

We next constructed a protein interaction map for 258 genes of the 282set based on a binary or an "all by all" yeast two-hybrid (Y2H) approach (**Table S1**). Because ABA receptor-PP2C interactions are ABA-dependent in yeast, all Y2H assays were performed in both the presence and absence of ABA to determine if any of the 66,564 potential PPIs were dependent on ABA (Park et al., 2009). Therefore, this study represented a comprehensive analysis of ABA-dependent interactions. Larger scale Y2H analysis is often performed in series where autoactivating proteins are first identified using one reporter system and then all subsequent interactions are retested using a different reporter system (Yu et al., 2008). We found, however,

that protein autoactivation frequently depended on the reporter assay, thus performing Y2H assays in series could result in a sampling bias that eliminates potential interactions only found in one reporter system. To reduce reporter bias, we performed Y2H assays using two reporter outputs in parallel. Although it is relatively easy to score interactions involving a colorimetric output (X-gal), the quantification of outputs based on yeast growth (growth in the absence of leucine) required the development of an imaging algorithm (DataEater) that did not require high-resolution images of yeast colonies (**Supplemental Experimental Procedures**). DataEater automatically generated a table of pixel intensities for each colony as a relative quantification of yeast growth. Using these values in combination with the X-gal data, we devised a simple generative model that assigned confidence values for each interacting pair, which led to a list of 512 statistically significant PPIs involving 138 gene nodes. (**Supplemental Experimental Procedures**, **Table S1**). This set of interactions represents approximately 0.8% of the possible interaction space.

The TRAIN contains genes that have functions in diverse processes ranging from metabolism and proteolysis to signaling and transcription (**Figure 1C**). A force-directed representation of the TRAIN in which proteins with similar interacting partners are more proximal whilst proteins with less similar interactions are positioned further apart, revealed a dense cluster of protein interactions (**Figure 1C**). Gene ontology (GO) annotation suggested this cluster was enriched for proteins that localize in the nucleus, many of which are TFs. Furthermore, this dense region also contained a number of core ABA signaling components including PYL receptors, PP2Cs and ABFs, all of which are thought to have roles in the nucleus. Thus, many of the PPIs identified were not only ABA-dependent for co-expression but also encoded nuclear proteins. Enrichment in protein pairs annotated with common gene ontology is a common criterion for high quality and

biologically significant interactome data sets (Stelzl et al., 2005). In summary, the TRAIN fulfills many of the standard validation requirements commonly used in interactome studies.

The eTRAIN

The TRAIN is obviously not an exhaustive network since it is biased towards ABA-regulated gene expression. We therefore expanded the interactome by querying TRAIN proteins against three large protein interactome databases and a collection of literature curated interactions (*Arabidopsis* Interactome Mapping Consortium, 2011; Lalonde et al., 2010; Popescu et al., 2009). This analysis, which expanded the TRAIN to a network of 573 proteins that encompassed 1008 interactions, was designated the eTRAIN (**Figure 2**). The eTRAIN not only demonstrated the complex relationship of ABA signaling with respect to diverse biological processes but also suggested potential interplay between ABA and these other processes. For example, 31 genes within the eTRAIN were GO annotated as having roles in other hormone signaling pathways and these nodes show approximately 100 interactions within the eTRAIN (**Figure 2)**. These hormone-based nodes may act as points of crosstalk that help coordinate ABA with other hormonal responses.

Core ABA signaling network

Presently, core ABA signaling is composed of thirteen PYL receptors, nine PP2Cs, three SNRK2s and five ABF transcriptional activators (Cutler et al., 2010; Hubbard et al., 2010). The TRAIN consists of three *PYL* receptors (*PYR1, PYL4, PYL8*), four *PP2Cs* (*ABI1, AHG3, HAB1, HAI1*), two *ABFs* (*ABI5, ABF3*) but not *SNRK2* kinases, because the latter are not induced by ABA addition (Fujita et al., 2009; Fujii and Zhu, 2009). Of the 12 possible TRAIN related PYL-

PP2C interactions, 11 were recapitulated and no other interactions were found to be ABA-dependent (**Figure S2**). We also identified previously reported interactions (PYL8/MYB77, ABI5/AFP2, ABI5/AFP4), which suggested that our interaction conditions and statistical filtering were of high quality (*Arabidopsis* Interactome Mapping Consortium, 2011; Garcia et al., 2008).

In addition to these published interconnections, interactions among core proteins were identified between PP2Cs (ABI1/HAI1, AHG3/HAI1) and between PP2Cs and ABFs (ABI1/ABI5, HAI1/ABI5) (**Figure 3A**). These interactions are consistent with recent reports of interactions and direct dephosphorylation of select ABFs by various PP2Cs (Lynch et al., 2012). We also uncovered additional connections between the PYL8 receptor and the TFs, MYB49 and a bHLH (At1g10585), which we have designated as AIB1 for ABA-induced basic helix-loop-helix (**Figure 3A**). Other PP2C interactions with kinases (SNRK3.15, SNRK3.22, MAP3K∂4), a phosphatase (SSP4), and a large set of TFs, metabolic enzymes and proteins of unknown function, were identified (**Figure 3A**). The PP2C interactions with SNRK3.15 and SNRK3.22 adds to the large number of core PP2C-SNRK3 family interactions that already exist in the literature and further support the interplay between these ABA regulated phosphatases and these calcium regulated kinases (Batistič et al., 2012; Coello et al., 2011). Finally, ABFs were found to interact with the following: two kinases (MAP3K∂4, WNK2), a phosphatase (SSP4), seven TFs (ANAC19, ANAC32, ANAC72, ERF58, CIR1, MYB49, AIB1) and a collection of proteins involved in metabolism and unknown functions (**Figure 3A**).

Functional analysis using sensitivity to ABA as a phenotype has been useful in classifying genes as positive or negative regulators of the overall ABA response. Presently, literature curation of the components that touch core signaling proteins indicate eight genes encode

positive regulators and 14 are negative (**Figure 3A**). To expand this functional analysis, we arbitrarily identified loss-of-function mutations for 16 TRAIN genes that interacted with core PP2Cs and determined their ABA sensitivity at the level of germination and cotyledon expansion (**Figure 3B**). Among the TRAIN genes, *myb12, athb12, erf58*, *rap2.2* and *map3k∂4* all showed increased sensitivity to ABA suggesting they encode negative regulators of the ABA response. The ABA hypersensitivity of *athb12* is consistent with other studies (Valdés et al., 2012). In addition, the *myb12* triple mutant containing another *myb12* allele in combination with loss-of-function mutations in its closest homologs (*myb12 myb11 myb111)* resulted in an ABA hypersensitive phenotype (**Figure 3B**). MYB12 has been implicated as a positive transcriptional regulator of flavanol synthesis (Stracke et al., 2010). This additional ABA-related phenotype suggests this TF impinges on both pigment and hormone signaling. Finally, we assayed the effects of *ERF058, RAP2.2* and MAP3K∂4 on ABA sensitivity by constructing transgenic lines that conditionally misexpressed these genes. We found that Dexamethasone (DEX)-inducible gain-of-function lines for all three transgenics were less sensitive to ABA in the presence of DEX (**Figure 3B**). These results suggest these genes were both necessary and sufficient negative regulators of ABA responsiveness.

In summary, over 50 interactions to core components have been added from the TRAIN to approximately 60 PPIs curated from literature. Interestingly, 20 of these interactions included a member in one of six TF families (*MYB, HB, DELLA, ANAC, ERF, bHLH*). By contrast, only the B3 domain TF, ABI3, has been reported to interact with an ABA core component outside of the ABFs (Nakamura et al., 2001). Thus, the conditions used in this study appeared to enrich for TF based interactions that are missed by other high and low throughput interaction studies. Finally, no loss- or gain-of-function lines tested in this study uncovered a positive regulator of ABA

response. Previous studies indicate that many genes that interact with core signaling components encode negative regulators of the ABA response (**Figure 3A**; **Table S1**). TRAIN-related signaling components, for which an ABA related phenotype could be identified, appear to add to this list of negative regulators.

A SNRK3 network that impinges on ABA responsiveness

One of our goals in developing a meso-scale ABA signaling network was to generate an experimentally tractable system in order to identify signaling modules. To test this hypothesis, we decided to focus on a sub-network centered around two kinases, SNRK3.15 and SNRK3.22, which formed two large and overlapping hubs (**Figure 4A**). The SNRK3 family is of particular interest because members of this group in Arabidopsis are implicated in a myriad of plant metabolic and stress responses (Batistič et al., 2012; Coello et al., 2011). Moreover, a number of related SNRK3 proteins interact with known core PP2Cs, ABI1 and ABI2, suggesting that these kinases crosstalk to the core ABA signaling pathway (Batistič et al., 2012; Ohta et al., 2003). Finally, higher resolution interaction mapping (**Supplemental Experimental Procedures**) revealed that SNRK3 interactions were significantly enriched for TFs compared to other types of partners (Fisher's exact test, $p < 2.8 \times 10^{-6}$) (**Figure 4A**). Moreover, many of the TF partners of SNRK3 interacted with each other, often resulting in three or four node interaction motifs that are indicative of signaling modules (Zhang et al., 2005).

We used Bimolecular Fluorescence Complementation (BiFC) assays in *N. benthamiana* to validate a large number of SNRK3 interactions *in planta* (Walter et al., 2004). Based on 22 Y2H results that included both presence and absence of SNRK3-dependent interactions, 17 (77%) were recapitulated *in planta* (**Figures 4B** and **S3A-D**). Green and blue lines indicate Y2H

interactions that were recapitulated and not recapitulated by BiFC analysis, respectively. We then decided to study a number of SNRK3-TF interactions in more detail by monitoring protein modification using two-dimensional gel shift assays in yeast. We found that the following TFs, ATHB6, MYB49, RGL3, ERF058, RAP2.2 and ANAC018, showed shifts in charge and size consistent with protein phosphorylation when co-expressed with a SNRK3 in yeast as indicated by green lines (**Figures 4C** and **S4A**). Blue lines denote the absence of a shift. Finally, both SNRK3s phosphorylated RAP2.2, ATHB6 and ANAC18 *in vitro*, which suggested that these TFs are direct downstream targets of SNRK3s (**Figures 4D** and **S4B**). In summary, the level of reproducibility between the yeast- and plant-based assays indicated that many SNRK3-dependent interactions are of high quality. More importantly, interactions gleaned from the TRAIN could be used as a guide in biochemical based experiments to identify direct targets of SNRK3.15 and/or SNRK3.22.

Our analysis of the SNRK3.15/SNRK3.22 sub-network suggested these kinases form a signaling module that may have roles in the plant's overall ABA response. A key tenet of a signaling module specifies that perturbing modular components often result in similar phenotypes (Hartwell et al., 1999). SNRK3.22 is a key regulator of a plasma membrane H^+-ATPase function but there is little suggestion of a role for this kinase in ABA-mediated transcription (Fuglsang et al., 2007). Functional analysis of SNRK3.15 suggests this gene is a negative regulator of ABA response but paradoxically loss of SNRK3.15 decreases expression of common ABA response genes in the presence of ABA (Qin et al., 2008). The TRAIN suggested these kinases should function in related processes that should connect to ABA based transcription. To explore this possibility, we first analyzed both loss- and gain-of function alleles of these genes with respect to ABA sensitivity. We found that loss-of-function alleles in both kinases had increased sensitivity

to ABA versus wild type (**Figure 4E**). Consistent with this, DEX inducible gain-of-function lines for both of the SNRK3s were less sensitive to ABA in the presence of DEX (**Figure 4E**). Therefore, *SNRK3.15* and *3.22* were both necessary and sufficient negative regulators of ABA responsiveness. Next, to clarify the role of SNRK3.15 in ABA-mediated transcription, we activated *SNRK3.15* in our DEX-inducible SNRK3.15 seedlings by DEX addition and monitored genome-wide transcription after ABA treatment (**Figure S5**). After filtering the data for consistency of expression, approximately 200 genes showed a two-fold change in expression upon ABA addition in the absence of SNRK3.15 activation (**Table S2**). Of these, 141 genes were misexpressed in the *snrk2* triple mutant, thus 70% of the ABA-responsive genes in our data set are influenced by core ABA signaling (Fujita et al., 2009). Upon activation of SNRK3.15, transcription of many of these ABA-responsive genes was attenuated (**Figure 4F**). This result is consistent with our functional analysis and suggests the SNRK3.15/SNRK2.22 hub plays a role in dampening transcription dependent on core ABA signaling.

Integrative mapping of the TRAIN by co-expression analysis identifies putative abiotic modules

Whole genome expression analysis has been used extensively to dissect the role of ABA in the overall response of plants to various stresses such as drought, salt and temperature (Kilian et al., 2007; Cramer et al., 2011; Zeller et al., 2009). However, animal studies have demonstrated that the performance of transcriptome data as a diagnostic tool of particular processes is greatly improved when expression data is mapped onto protein interaction maps (Taylor et al., 2009; Chuang et al., 2007). This is particularly true when data integration focuses on proteins with many interacting partners ("hubs") as hubs are critical to network conductivity (Fraser, 2005;

Han et al., 2004). We therefore decided to combine transcriptome data garnered from a variety of abiotic stresses with the TRAIN to see if dynamic patterns of network wiring emerge in response to particular stresses.

Rather than simply overlaying the magnitude of expression of TRAIN genes during a specific time or stress condition onto TRAIN nodes, we calculated a Pearson correlation coefficient (PCC) of co-expression for each pair of interacting proteins within the TRAIN, across multiple time points for both shoots and roots upon individual stresses. A PCC value above 0.75 reflected high co-expression between the partners whilst values below -0.75 meant the gene pair is anti-correlated in expression. For example, co-expression analysis based on osmotic stress expression data from combined root and shoot tissues over 12 timepoints from AtGenExpress, generated average PCC values between PYL4 and its PP2C partners of -0.9766 (HAB1), -0.849 (ABI1), -0.8833 (HAI1) and -0.8378 (AHG3) (Kilian et al., 2007). These highly negative correlations are consistent with the diametrically opposed expression of these genes in the presence of ABA.

To evaluate TRAIN co-expression analysis versus standard representations of gene expression globally, we first generated heat map representations of TRAIN gene expression over the same various abiotic stresses and times (**Figure 5A**). Osmotic, salt and cold stress all showed related patterns of gene expression with osmotic and salt being the most similar. However, although osmotic and salt have similar heat map expression patterns, their TRAIN co-expression maps showed clear differences (**Figure 5B**). The HAI1 hub, for example, was highly correlated with the expression of many of its partners in both osmotic and salt stress datasets. But the hub protein MAP3k∂4 only correlated well with its partners under osmotic stress whilst AIB1 highly correlated with its partners in salt stress (**Figure 5B**). Neither *MAP3K∂* nor *AIB1* have been

extensively studied but these results suggest these genes may be associated with these particular stresses.

To explore this possibility in detail, we examined the AIB1 subnetwork. The AIB1 hub represents 55 partners many of which show highly correlated expression with AIB1 under salt stress conditions (**Figure 6A**, **Table S1**). Many of the AIB1 partners that show salt dependent co-expression are annotated as having roles within the nucleus. After limiting partner interactions to TFs, an AIB1 centered complex, which comprised of ATHB12 and a collection of ANAC and MYB TFs, emerged (**Figure 6A**). By comparison, similar co-expression analysis based on osmotic expression data did not predict these AIB1 complexes (**Figure 6A**). By contrast, co-expression analysis identified an osmotic related complex consisting of ABI5, AFP2 and ATHB12, which were not supported under salt stress conditions (**Figure 6A**). This analysis suggested different nuclear complexes may coalesce in response to different abiotic stresses and that AIB1 might be a key component of a transient nuclear complex that functions in salt homeostasis. Unfortunately, loss-of-function mutations in the *AIB1* gene are not publically available to test its function. Thus, we constructed DEX-inducible gain-of-function *AIB1* lines and tested them for osmotic- and salt-related phenotypes. The presence of DEX did not influence the growth response of *AIB1* transgenic seedlings to increasing osmotic stress (**Figure 6B**). By contrast, DEX induction of *AIB1* in transgenic plants did confer an increased sensitivity to salt that was not observed in the absence of DEX, which suggested *AIB1* has a negative role in salt homeostasis (**Figure 6B**). These results suggest changes in modularity as monitored by changes in co-expression of protein partners, may improve the predictive value of interactomes for designing function experiments.

DISCUSSION

We have developed a systems-based strategy to define a signaling landscape for the plant hormone ABA. Our approach was centered on the premise that proteins contributing to the ABA signaling network will often be co-expressed and should interact at some point to transduce signaling information. Unlike many ABA based transcriptome studies, we limited our conditions to low levels of ABA and a short duration of exposure to ABA in order to enrich for primary transcriptional events. This resulted in only a few hundred genes whose expression appeared to be regulated mostly by core ABA signaling. This relatively small number of genes allowed meticulous experimental, statistical and annotation analysis of our protein interaction space to give a high quality ABA regulated network of over 500 interactions. Our approach confirmed many core ABA signaling interactions and linked core components to over 50 additional protein partners many of which represent various transcriptional factor families. The meso-scale nature of the TRAIN also allowed systematic functional analysis of specific signaling modules. And finally, mapping co-expression correlation onto the TRAIN allowed prediction of genes and signaling modules that may play important roles in specific ABA related abiotic stresses.

Although the TRAIN is an attempt to define a comprehensive ABA signaling network, there are several constraints to our approach. First, it is expected that ABA does not transcriptionally regulate many important genes that contribute to its signaling network. For example, the core SNRK2s involved in ABA signaling are not regulated by ABA addition (Fujita et al., 2011). With this in mind, we merged the TRAIN with literature curated protein interactions (*Arabidopsis* Interactome Mapping Consortium, 2011; Lalonde et al. 2010; Popescu et al. 2008). This eTRAIN doubled the number of interactions and contained proteins that have been belong to over 30 GO annotated functions. Interestingly, although literature curation doubled the size of the

interactome, one gene, encoding a LEA protein (At1g65690), actually accounted for over 200 of these additional interactions. Removal of these LEA interactions meant that only 384 interactions out of the 30,000 confirmed PPIs reported for Arabidopsis were added to the TRAIN. Moreover, there was little interaction space overlap between the TRAIN and those published for high-throughput studies. These differences may reflect the experimental limitations that are inherent to high-throughput systems and analysis of high-throughput plant interactomes suggests these approaches have likely captured only 10% of the possible interactions (Chen et al., 2010, *Arabidopsis* Interactome Mapping Consortium, 2011). By contrast, the medium size of the TRAIN space allows for multiple testing of interactions with different vectors and reporter output systems, which has been shown to be an essential benchmark for quality control in Y2H systems (Chen et al., 2010). The finding that 70% of our Y2H interactions could be recapitulated *in planta* further supports the experimental and statistical approaches used here to build our interaction network. Whatever the case, the focused approach of this study on a particular process like hormone signaling, is essential in filling out the larger scale interaction maps built by high-throughput methods.

A second limitation of our approach was the use of a specific duration and amount of ABA added, thus limiting our transcriptome analysis to only one stage of development. A recent comprehensive comparison of ABA regulated transcriptome experiments found few genes in common among 14 datasets (Wang et al., 2011). Although this most likely reflects the differences in ABA concentrations, tissues and developmental stages used in these experiments, it also demonstrates the flexibility of ABA-related transcriptional response during the life cycle of a higher plant. Thus, a comprehensive ABA network will likely require a number of spatial- and temporal-based "TRAIN like" interactomes. The TRAIN could also be reduced to the

resolution of a single cell, based on the integration of cell-type specific interaction and expression data. This microscopic level of analysis was not possible prior to the TRAIN and would likely lead to valuable insight into the mechanisms of how different cell types respond to ABA.

It is notable that functional analysis of the TRAIN uncovered only negative regulators of ABA-mediated signaling. This could mean the transcriptome assay conditions used to identify TRAIN genes enriched for negative regulators. However, we think this is unlikely since two thirds of the genes curated from the literature that link to the core ABA signaling pathway and show ABA related phenotypes, also appear to attenuate the ABA response. This attenuation of the core ABA signaling pathway could reflect a negative feedback response to the initial activation of the core pathway by ABA.

With respect to the ABA signaling network, a large number of kinases annotated as being involved in calcium mediated signaling, appeared to interact with core ABA signaling components and PP2Cs in particular. Within the TRAIN there were three major kinase hubs, a MAP3K∂4 and two SNRK3s. Regarding SNRK3.15 and SNRK3.22, our analysis indicated these kinases act as negative regulators of the ABA response, which is opposite to the SNRK2 kinases involved in core ABA signaling (Fujita et al., 2009; Fujii and Zhu, 2009). Interestingly, it appears that a number of TFs interacting with SNRK3(s) including ones shown to be phosphorylated by either SNRK3.15 or SNRK3.22, were also negative regulators of the ABA response. This could mean these kinases and a number of their TF targets may form a signaling module. At this time, it is not clear how these SNRK3s coordinate with core SNRK2s to modulate the overall ABA response. SNRK3 transcription is dependent on SNRK2 activation, thus each kinase group is temporally separated. Furthermore, the absence of SNRK3 interactions with either ABI5 or ABF3 suggests a separation between the TFs regulated by SNRK2s in the

core pathway and TFs targeted by SNRK3s. Interestingly, a number of TF partners of SNRK3 interacted with the central ABA signaling transcriptional regulator ABI5 (Lopez-Molina et al., 2001; Lopez-Molina et al. 2002). Possibly, ABI5 may act as a common point of crosstalk between SNRK2 and SNRK3 signaling.

Although little is known about the targets of SNRK3.15 signaling, SNRK3.22 does negatively regulate the activity of the AHA2 plasma membrane H^+-ATPase through phosphorylation (Fuglsang et al., 2007). The control of PM H^+-ATPase by SNRK3.22 regulates intracellular pH homeostasis in response to alkaline pH, which in turn modulates the plant's overall response to salt stress under alkaline conditions. Apart from its role in membrane-based salt homeostasis, we found that one target of SNRK3.22, a bHLH transcription factor AIB1, is also connected to a salt stress response. Notably, many SNRK3.15 (24/26) and SNRK3.22 (22/23) interactors also partner with AIB1 (**Figure S6**). Thus, SNRK3.22 and perhaps SNRK3.15 may act as central coordinators in response to salt stress at both the plasma membrane and the nucleus.

In conclusion, it is believed that most signaling modules are meso-scale encompassing 25-100 proteins (Spirin and Mirny, 2003). The experimental conditions used in this study, which result in an interaction space around approximately 100 proteins, was ideal in capturing a network of this scale. Our network was simple enough to identify modules that could be probed functionally. More importantly, unlike other plant studies that identify sub-networks through functional analysis or gene expression signatures alone, the overlaying of co-expression onto the TRAIN led to the identification of dynamic sub-networks based on changes in network wiring. These changes in sub-networks can be used to determine functional roles for hubs and specific signaling modules. We believe this approach of merging co-expression onto protein interaction networks will have important predictive value in assigning gene function. On this note, the approaches

used here should be readily applicable to other meso-scale signaling processes such as pathogen infection or growth on different nutrient conditions. These approaches would also be advantageous in dissecting non-model plant and animal processes where genetic tools are not readily available.

EXPERIMENTAL PROCEDURES

Plant material and growth conditions

All Arabidopsis strains used in this study were of the ecotype Columbia (Col-0). See **Supplemental Experimental Procedures** for details.

Construction of the Transcriptionally Regulated ABA Interactome Network (TRAIN)

Sterile seeds were placed on 1/2X MS plate and imbibed for four days at 4°C. Plates were transferred to room temperature under continuous white light for 11 days. Eleven day old seedlings were moved to 1/2X MS plates (10 μM cycloheximide ±1 μM ABA) for 6 hours. Total RNA was processed and hybridized on a GeneChip *Arabidopsis* ATH1 genome array. Duplicate samples were analyzed for each condition. See **Supplemental Experimental Procedures** for construction of the TRAIN.

Protein Purification and Kinase Assays

Kinase reactions were conducted in 20 uL of kinase buffer with 1μCi [γ^{32}P]ATP for 15 minutes at room temperature and terminated by adding Laemmli buffer. Reactions were loaded onto 12% SDS-PAGE gels, and incorporated radiolabel was visualized by autoradiography. Kinase assays

were run on SDS-PAGE gels and visualized by Coomassie blue staining. See **Supplemental Experimental Procedures** for details.

Yeast Expression and 2D Gel Analysis

Streaked haploid EGY48 yeast expressing the various transcription factors in the pJG4-5 vector, or diploid yeast (EGY48 / RFY206) co-expressing individual transcription factors and kinases in the pJG4-5 and pEG202 vectors, respectively, were resuspended from YNB plates to 0.1 OD600 in 3 ml of appropriate YNB galactose drop-out media to induce protein expression. Cultures were grown overnight at 30 °C. Pellets were solubulized with glass beads in 200 μL of the rehydration buffer (Bio Rad, Hercules, CA) and 75 μg of each protein sample was absorbed into 7 cm IPG (pH 3-10) strips and separated in the 1st dimension by the Protean IEF Cell as per manufacturer's instructions (Bio Rad, Hercules, CA). The IPG strips were processed and the proteins separated in the second dimension by 12 % SDS-PAGE. Following electrophoresis, the transcription factors were detected by immunoblot analysis using HA antibodies (Roche; 1/15000).

Bimolecular fluorescence complementation (BiFC) analysis

BiFC and split YFP fusions were transiently expressed using *Agrobacterium tumefaciens* in *N. benthamiana* as described (Walters et al., 2004). The *A. tumefaciens* strain GV2260 (final density of 0.2 OD600) was used to syringe-infiltrate *N. benthamiana* leaves. YFP was visualized using standard techniques on the confocal, Leica TCS SP5.

Microarray analysis of DEX inducible *SNRK3.15* lines

Stratified seeds were transferred to room temperature under continuous white light for 4 days and then transferred to either to a 0.1% DMSO or a 30μM DEX plate (24 h). After this incubation, seeds were transferred to 0.1% DMSO or 2μM ABA ±30μM DEX for 24 hours. RNA was analyzed by hybridization on a GeneChip *Arabidopsis* ATH1 genome array. See **Supplemental Experimental Procedures**.

Gene Expression Analysis

Gene expression data was generated from the AtGenExpress global stress expression data set downloaded from the BAR http://dx.doi.org/10.1111/j.1365-313X.2005.02437.x) or from GEO (Toufighi, K. et *al* 2005). The expression platform used in all cases was the ATH1 GeneChip from Affymetrix. The data sets and comparisons were as follows: *aba2-2* seedlings one comparison: 6 hr with 1 μM ABA vs. mock-treated plant; http://bar.utoronto.ca/affydb/cgi-bin/affy_db_proj_viewer.cgi?proj=26&view=general. Heatmaps of abiotic stress transcription were generated using GENE-E (http://www.broadinstitute.org/cancer/software/GENE-E/index.html). Pearson correlation coefficients (PCC) between each protein pair within the TRAIN was generated over each abiotic stress using AtGenExpress global stress expression data set expression data from both roots and shoots over six time periods.

SUPPLEMENTAL INFORMATION

Methods and any associated references are available in Supplemental Information

ACKNOWLEDGEMENTS

We thank Dr. E. Nambara for helpful discussion. We also thank the Ohio State Stock Center, Salk Institute Genomic Analysis Laboratory (SIGnAL) for providing materials as well as Dr. N. Nishimura for *ahg3-1* seed and Dr. Bernd Weisshaar for *myb12* and *myb12 myb11 myb111* triple mutant seed.

REFERENCES

Arabidopsis Interactome Mapping Consortium (2011). Evidence for Network Evolution in an Arabidopsis Interactome Map. Science *333*, 601-607.

Batistič, O., Rehers, M., Akerman, A., Schlücking, K., Steinhorst, L., Yalovsky, S., Kudla, J. (2012). S-acylation-dependent association of the calcium sensor CBL2 with the vacuolar membrane is essential for proper abscisic acid responses. Cell Res. *22*, 1155-1168.

Batistič, O. and Kudla, J. (2012). Analysis of calcium signaling pathways in plants. Bio. Biophy. Acta *1820*, 1282-1293.

Ben-Ari, G. (2012). The ABA signal transduction mechanism in commercial crops: learning from Arabidopsis. Plant Cell Rep. *31*, 1357-1369.

Brandt, B., Brodsky, D.E., Xue, S., Negi, J., Iba K., Kangasjarvi, J., Ghassemian, M., Stephan, A.B., Hu, H., and Schroeder J.I. (2012). Reconstitution of abscisic acid activation of SLAC1 anion channel by CPK6 and OST1 kinases and branched ABI1 PP2C phosphatase action. Proc. Natl. Acad. Sci. USA *109*, 10593–10598.

Chen, Y.C., Rajagopala, S.V., Stellberger, T., Uetz, P. (2010). Exhaustive benchmarking of the yeast two-hybrid system. Nat Methods. *7*, 667-668.

Chuang, H.Y., Lee, E., Liu, Y.T., Lee, D., and Ideker, T. (2007). Network-based classification of

breast cancer metastasis. Mol. Syst. Biol. *3*, 140.

Cutler, S.R., Rodriguez, P.L., Finkelstein, R.R., and Abrams, S.R. (2010). Abscisic acid: emergence of a core signaling network. Ann. Rev. Plant Biol. *61*, 651–79.

Coello, P., Hey, S.J., and Halford, N.G. (2011). The sucrose non-fermenting-1-related (SnRK) family of protein kinases: potential for manipulation to improve stress tolerance and increase yield. J. Exp. Bot. *62*, 883–893.

Cramer, G.R., Urano, K., Delrot, S., Pezzotti, M., and Shinozaki, K. (2011). Effects of abiotic stress on plants: a systems biology perspective. BMC Plant Biol. *11*, 163.

Fraser, H.B. (2005). Modularity and evolutionary constraint on proteins. Nat. Genet. *37*, 351–352.

Fuglsang, A.T., Guo, Y., Cuin, T.A., Qiu, Q., Song, C, Kristiansen, K.A., Bych, K., Schulz, A., Shabala, S., Schumaker, K.S., et al. (2007). Arabidopsis protein kinase PKS5 inhibits the plasma membrane H+ -ATPase by preventing interaction with 14-3-3 protein. Plant Cell. *19*, 1617-1634.

Fujita Y., Nakashima, K., Yoshida, T., Katagiri, T., Kidokoro, S., Kanamori, N., Umezawa, T., Fujita, M., Maruyama, K., Ishiyama, K., et al. (2009). Three SnRK2 protein kinases are the main positive regulators of abscisic acid signaling in response to water stress in Arabidopsis. Plant Cell Physiol. *50*, 2123–2132.

Fujita, Y., Fujita, M., Shinozaki, K., and Yamaguchi-Shinozaki, K. (2011). ABA-mediated transcriptional regulation in response to osmotic stress in plants. J. Plant Res. *124*, 509–525.

Fujii, H. and Zhu, J.-K. (2009). Arabidopsis mutant deficient in 3 abscisic acid-activated protein kinases reveals critical roles in growth, reproduction, and stress. Proc. Nat. Acad. Sci. USA *106*, 8380–8385.

Garcia, M. E., Lynch, T., Peeters, J., Snowden, C. and Finkelstein, R. (2008). A small plant-specific protein family of ABI five binding proteins (AFPs) regulates stress response in germinating Arabidopsis seeds and seedlings. Plant Mol. Biol. *67*, 643–658.

Ge, H., Liu, Z., Church, G.M., and Vidal, M. (2001). Correlation between transcriptome and interactome mapping data from *Saccharomyces cerevisiae*. Nature Gen. *29*, 482-486.

Geiger, D. Maierhofer, T., Al-Rasheid, KA., Scherzer, S., Mumm, P., Liese, A., Ache, P., Wellmann, C., Marten, I., Grill, E., *et al*. (2011). Stomatal closure by fast abscisic acid signaling is mediated by the guard cell anion channel SLAH3 and the receptor RCAR1. *Sci Signal*. 17, ra32.

Han, J.D., Bertin, N., Hao, T., Goldberg, D.S., Berriz, G.F., Zhang, L.V., Dupuy, D., Walhout, A.J., Cusick, M.E., Roth, F.P., *et al*. (2004). Evidence for dynamically organized modularity in the yeast protein protein interaction network. Nature *430*, 88–93.

Hartwell, L.H., Hopfield, J.J., Leibler, S., and Murray, W. (1999). From molecular to modular cell biology. Nature *402*, C47-52.

Hey, S.J., Byrne, E. and Halford, N.G. (2010). The interface between metabolic and stress signalling. Ann. of Bot. *105*, 197–203.

Huang, G.T., Ma, S.L., Bai, L.P., Zhang, L., Ma, H., Jia, P., Liu, J., Zhong, M., and Guo, Z.F. (2012). Signal transduction during cold, salt, and drought stresses in plants. Mol. Biol. Rep *39*, 969–987.

Hubbard, K.E., Nishimura, N., Hitomi, K. Getzoff, E.D., and Schroeder, J.I. (2010). Early abscisic acid signal transduction mechanisms: newly discovered components and newly emerging questions. Genes & Dev. *24*, 1695–1708.

Kilian, J., Whitehead, D., Horak, J., Wanke, D., Weinl, S., Batistic, O., D'Angelo, C., Bornberg-Bauer, E., Kudla, J., Harter, K. (2007). The AtGenExpress global stress expression data set: protocols, evaluation and model data analysis of UV-B light, drought and cold stress responses. Plant J. *50*, 347–363.

Lalonde, S., Sero, A., Pratelli, R., Pilot, G., Chen, J., Sardi, M.I., Parsa, S.A., Kim, D.Y., Acharya, B.R., Stein, E.V. et al. (2010). A membrane protein/signaling protein interaction network for Arabidopsis version AMPv2. Front. Physiol. *1*, 1-24.

Léon-Kloosterziel, K.M., Gil, M.A., Ruijs, G.J., Jacobsen, S.E., Olszewski, N.E., Schwartz, S.H., Zeevaart, J.A., and Koornneef, M. (1996). Isolation and characterization of abscisic acid-deficient Arabidopsis mutants at two new loci. Plant J. *10*, 655-661.

Li, H.H., Hao, R.L., Wu, S.S., Guo, P.C., Chen, C.J., Pan, L.P., and Ni, H. (2011). Occurrence, function and potential medicinal applications of the phytohormone abscisic acid in animals and humans. Biochem Pharmacol. *82*, 701-712.

Lopez-Molina, L., Mongrand, S., and Chua, N.H. (2001). A postgermination developmental arrest checkpoint is mediated by abscisic acid and requires the ABI5 transcription factor in Arabidopsis. Proc Natl Acad Sci *98*, 4782-4787.

Lopez-Molina L., Mongrand S., McLachlin D.T., Chait B.T., and Chua N.H. (2002). ABI5 acts downstream of ABI3 to execute an ABA-dependent growth arrest during germination. Plant J. *32*, 317-328.

Lumba, S., Cutler, S., and McCourt, P. (2010). Plant nuclear hormone receptors: a role for small molecules in protein-protein interactions. Annu. Rev. Cell Dev. Biol. *26*, 445–469.

Lynch, T., Erickson, B.J., and Finkelstein, R.R. (2012). Direct interactions of ABA-insensitive (ABI)-clade protein phosphatase (PP2Cs) with calcium-dependent protein kinases and ABA

response element-binding bZIPs may contribute to turning off ABA response. Plant Mol. Biol. *80*, 647-58.

Nakamura, S., Lynch, T.J., and Finkelstein, R.R. (2001). Physical interactions between ABA response loci of Arabidopsis. Plant J. *26*, 627-635.

Nakashima, K., and Yamaguchi-Shinozaki, K. (2013). ABA signaling in stress-response and seed development. Plant Cell Rep. *32*, 959-970.

Ohta, M., Guo, Y., Halfter, U., and Zhu, J.-K. (2003). A novel domain in the protein kinase SOS2 mediates interaction with the protein phosphatase 2C ABI2. Proc. Nat. Acad. Sci. USA *100*, 11771-11776.

Park, S.Y., Fung, P., Nishimura, N., Jensen, D.R., Fujii, H., Zhao, Y., Lumba, S., Santiago, J., Rodrigues, A., Chow, T.F., Alfred, S.E., Bonetta, D., Finkelstein, R., Provart, N.J., Desveaux, D., Rodriguez, P.L., McCourt, P., Zhu, J.K., Schroeder, J.I., Volkman, B.F., Cutler, S.R. (2009). Abscisic acid inhibits type 2C protein phosphatases via the PYR/PYL family of START proteins. Science *324*, 1068–1071.

Popescu, S.C., Popescu, G.V., Bachan, S., Zhang, Z., Gerstein, M., Snyder, M., Dinesh-Kumar, S.P. (2009). MAPK target networks in *Arabidopsis thaliana* revealed using functional protein microarrays. Genes & Dev *23*, 80–92.

Qin, Y., L I, X., Guo, M., Deng, K., Lin, J., Tang, D., Guo, X., Liu, X. (2008). Regulation of salt and ABA responses by CIPK14, a calcium sensor interacting protein kinase in Arabidopsis. Sci China C. Life Sci. *51*, 391-401.

Spirin, V. and Mirny, L. (2003). Protein complexes and functional modules in molecular networks. Proc. Nat. Acad. Sci. USA *100*, 12123–12128.

Stelzl, U., Worm, U., Lalowski, M., Haenig, C. et al., (2005). A human protein–protein interaction network: a resource for annotating the proteome. Cell *122*, 957–968.

Stracke, R., Jahns, O., Keck, M., Tohge, T., Niehaus, K., Fernie, A.R., and Weisshaar, B. (2010). Analysis of PRODUCTION OF FLAVONOL GLYCOSIDES-dependent flavonol glycoside accumulation in *Arabidopsis thaliana* plants reveals MYB11-, MYB12- and MYB111-independent flavonol glycoside accumulation. New Phytol. *188*, 985-1000.

Taylor, I.W., Linding, R., Warde-Farley, D., Liu, Y., Pesquita, C., Faria, D., Bull, S., Pawson, T., Morris, Q., and Wrana, J.L. (2009). Dynamic modularity in protein interaction networks predicts breast cancer outcome. Nat. Biotechnol. *27*, 199-204.

Toufighi, K., Brady, S.M., Austin, R., Ly, E., and Provart, N.J. (2005). The Botany Array Resource: e-Northerns, Expression Angling, and promoter analyses. Plant J. *43*, 153-63.

Valdés, A.E., Overnäs, E., Johansson, H., Rada-Iglesias, A., and Engström, P. (2012). The homeodomain-leucine zipper (HD-Zip) class I transcription factors ATHB7 and ATHB12 modulate abscisic acid signalling by regulating protein phosphatase 2C and abscisic acid receptor gene activities. Plant Mol Biol. *80*, 405-418.

Van Leene, J., Boruc, J., De Jaeger, G., Russinova, E., and De Veylder, L. (2011). A kaleidoscopic view of the Arabidopsis core cell cycle interactome. Trend Plant Sci. *16*, 141-50.

Walter, M., Chaban, C., Schütze, K., Batistic, O., Weckermann, K., Näke, C., Blazevic, D., Grefen, C., Schumacher, K., Oecking, C., Harter, K., and Kudla, J. (2004). Visualization of protein interactions in living plant cells using bimolecular fluorescence complementation. Plant J. *40,* 428–438.

Wang, R.S., Pandey, S., Li, S., Gookin, T.E., Zhao, Z., Albert, R., Assmann, S.M. (2011). Common and unique elements of the ABA-regulated transcriptome of Arabidopsis guard cells. BMC Genomics. *12*, 216.

Wasilewska, A., Vlad, F., Sirichandra, C., Redko, Y., Jammes, F., Valon, C., Frei, D.F., and Leung, J. (2008). An update on abscisic acid signaling in plants and more... Mol. Plant *1*, 198–217.

Wilkinson, S., Kudoyarova, G.R., Veselov, D.S., Arkhipova, T.N., and Davies, W.J. (2012). Plant hormone interactions: innovative targets for crop breeding and management. J. Exp. Bot. *63*, 3499-3509.

Yu, H., Braun, P., Yildirim, M.A., Lemmens, I., Venkatesan, K., Sahalie, J., Hirozane-Kishikawa, T., Gebreab, F., Li, N., Simonis, N., et al. (2008). High-quality binary protein interaction map of the yeast interactome network. Science *322*, 104-110.

Zeller, G., Henz, S.R., Widmer, C.K., Sachsenberg, T., Ratsch, G., Weigel, D., and Laubinger, S. (2009). Stress-induced changes in the Arabidopsis thaliana transcriptome analyzed using whole-genome tiling arrays. Plant J. *58*, 1068-1082.

Zhang, L.V., King, O.D., Wong, S.L., Goldberg, D.S., Tong, A.H., Lesage, G., Andrews, B., Bussey, H., Boone, C., and Roth, F.P. (2005). Motifs, themes and thematic maps of an integrated Saccharomyces cerevisiae interaction network. J. Biol. *4*.

Figure 1. ABA signaling networks (A) Model of core ABA signaling pathway as defined by genetic analysis. An arrow indicates positive genetic interaction whilst a T-bar represents negative genetic interaction. (B) A comparison of the expression of the 282set in wild type seedlings exposed to 50μM ABA for 6 hours versus the *snrk2* (*snrk2.2/2.3/2.6*) triple mutant defective in core ABA signaling. The red dots are genes induced at least two-fold in the *aba2-2* mutant in response to ABA. Blue dots are genes repressed at least two-fold by ABA. Gene expression below the purple diagonal line are dampened in induction in the *snrk2* triple whilst genes above the diagonal line have increased expression. Graph axes are log-scale fold change. (C) An edge-weighted force-directed representation of the TRAIN. Node colour is designated by GO Slim Functional Annotation. Proteins with similar interaction profiles cluster more closely to each other. Line thickness represents edge-weighted confidence based on statistical analysis. See also **Figure S1** and **Table S1**.

Figure 2. An expanded map of ABA signaling protein-protein interactions (eTRAIN) Core ABA signaling components are represented by larger nodes at the upper center of the map whilst TRAIN components are represented by nodes in the middle ellipse. Core and TRAIN node component colors are designated by GO Slim Function annotation. Literature reported interactions are shown on the outside as orange nodes. Orange edges indicate interactions with core components. Categories shown on the outside are designated by GO Slim Function annotation. The list of genes and interactions can be found in **Table S1**.

Figure 3. Core ABA signaling network (A) A network of core ABA signaling pathway associations based on the TRAIN and literature curated interactions. A list of the genes, their

partners and their annotations can be found in **Table S1**. Grey edges represent previously published core ABA signaling interactions. Pink edges represent interactions found in this study. The ABA core signaling pathway is represented by larger black nodes and arrows. The list of phosphorylated proteins (orange balls) can be found in **Table S1**. The designation of positive and negative regulators in based on genetic analysis performed in this study or the literature. (B) Loss- and gain-of-function mutant analysis of select core component partners. Lines were tested on 0.7 μM ABA for hypersensitivity to ABA and 2.0 μM ABA for insensitivity. Three to six independent experiments were performed on each line using 50-100 seeds and similar results were obtained. The loss-of-function ABA hypersensitive mutant, *ahg3-1* and ABA insensitive *abi5-1* were used for comparison. For gain-of-function analysis, a strong DEX inducible line overexpressing *HAI1* was used. Data are represented as mean ± SD.

Figure 4. The SNRK3 network (A) The SNRK3.15-SNRK3.22 interaction network. Red connecting lines represent direct SNRK3.15 and SNRK3.22 partners and grey lines are other protein interactions. Line thickness indicates the edge-weighted confidence based on statistical analysis. Node size is proportional to the total number of interactions in the TRAIN dataset. (B) Summary of BiFC analysis of SNRK3.15 and SNRK3.22 interactions *in planta*. Green lines are Y2H interactions recapitulated by BiFC; Blue lines are Y2H interactions that were not recapitulated by BiFC analysis. See also **Figure S3A-D**. (C) Summary of two-dimensional gel analysis of TF mobility shifts in the presence of either SNRK3 in yeast. Green lines are SNRK3-dependent shifts, while blue lines denote the absence of a shift. See also **Figure S4A**. (D) *In vitro* phosphorylation by SNRK3s of a select number of TF targets. The band observed in the no TF lane is consistent with SNRK3 autophosphorylation. See also **Figure S4B**. (E) Loss- and

gain-of-function analyses of SNRK3.15 and SNRK3.22 lines. Conditions were similar to those presented in Figure 3B. Quantification of germination and cotyledon expansion of loss- and gain-of-function lines germinated on ABA are shown in lower graph. Data are represented as mean ± SD. (F) Transcriptome analysis of a DEX inducible SNRK3.15 line in the presence of ABA. Left lane, genes are filtered for those that showed at least a two-fold increase (red) or decrease (yellow) in the absence of DEX. See also **Figure S5** and **Table S2**. Right lane, expression of the two-fold gene set in the presence of SNRK3.15 activation. If the expression of an ABA induced gene is dampened it becomes more yellow whilst decreased expression of a repressed gene results in increased red color. Dotted grey line represents zero-fold baseline whilst the solid line represents the fold change for each gene.

Figure 5. Dynamic modularity of the TRAIN in response to different abiotic stresses (A) Heatmap representation of TRAIN gene expression in the shoot and root under different times of abiotic stress. The lower panel is a magnification of AIB1 expression. (B) Network graph of the TRAIN with interactions shown as edges that are colored according to the PCC of co-expression of partner proteins. Edge color indicates level of correlation between partner proteins with bluer edges indicating more correlated co-expression whilst redder edges represents more anti-correlation.

Figure 6. The AIB1 salt and osmotic sub-networks (A) Left panel, co-expression analysis of AIB1 partners under salt or osmotic stress. Middle panel, model of the AIB1 interaction network derived from TF partners. Edge color indicates level of correlation between partner proteins with bluer edges indicating more correlated co-expression whilst redder edges represent more anti-

correlation. Right panel, model of nuclear AIB1 complexes based on co-expression of partners. (B) Effects of mannitol (1 to 5%) and NaCl (25 to 300 mM) on DEX-inducible *AIB1* transgenic seedlings. Representative pictures are of seedlings grown in the absence (DMSO) or presence of mannitol (5%) or salt (50 mM NaCl) for 7 days. Bar = 1.0 mm.

Figure 1
Click here to download high resolution image

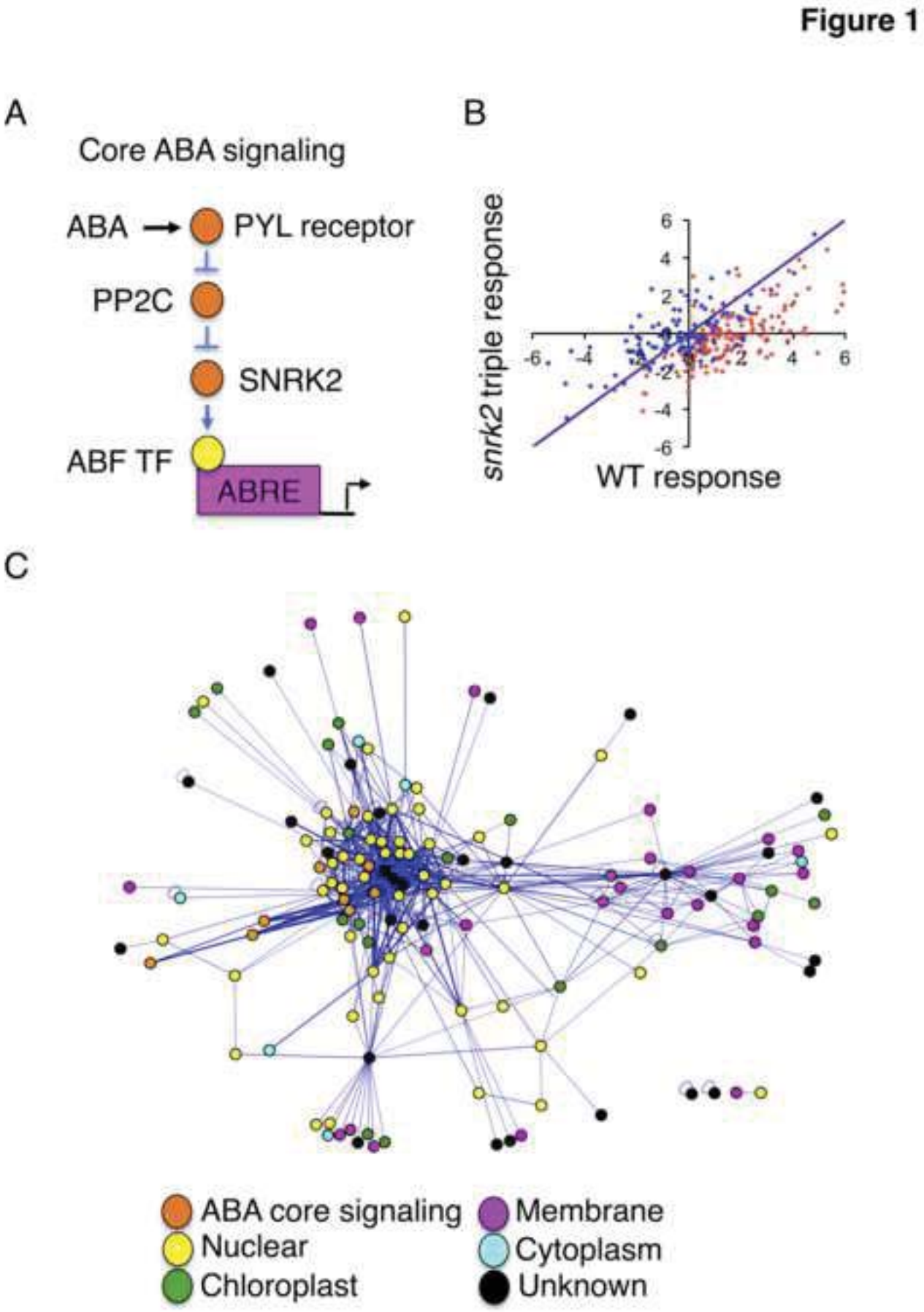

Figure 2
Click here to download high resolution image

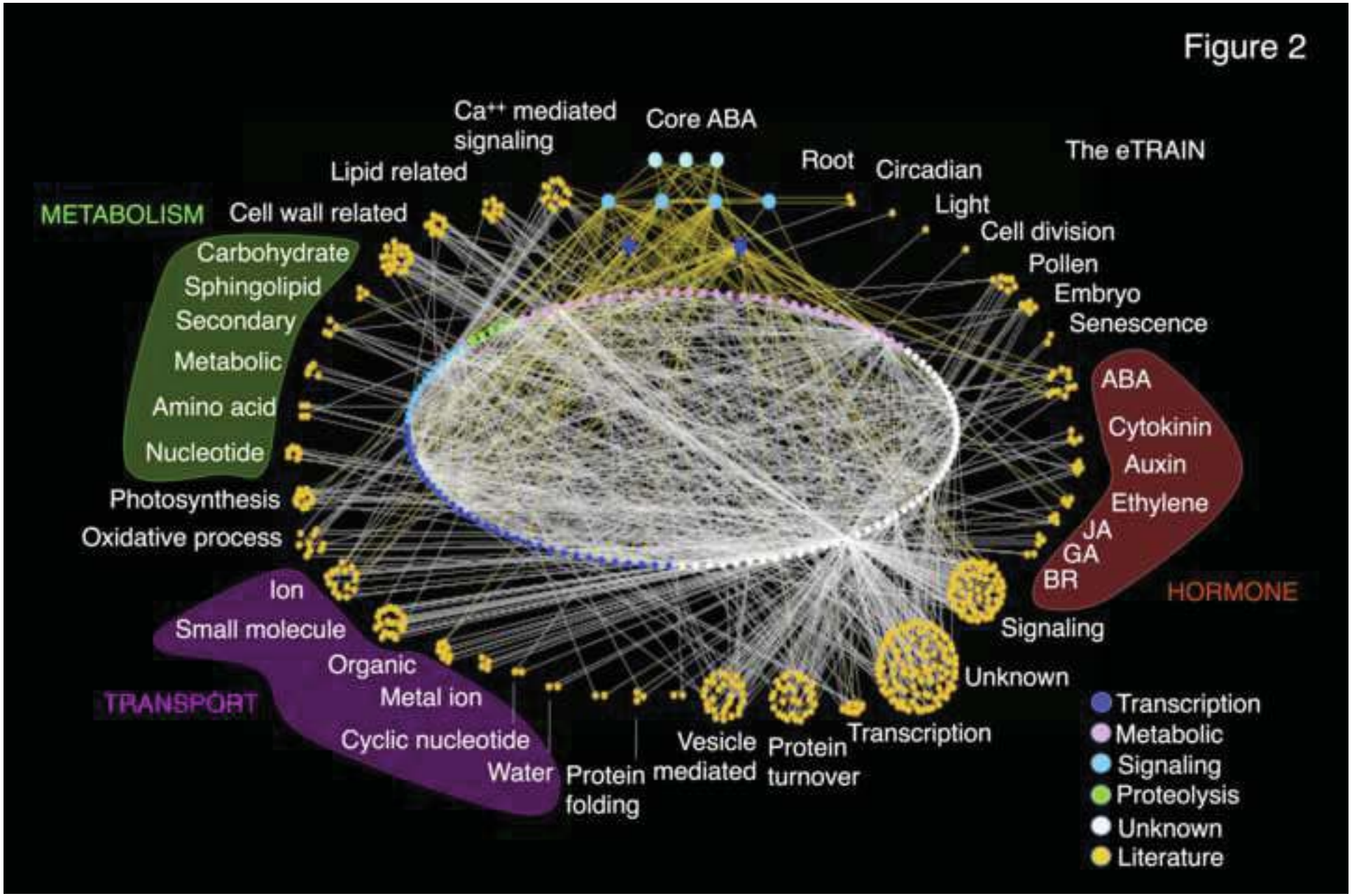

Figure 3
Click here to download high resolution image

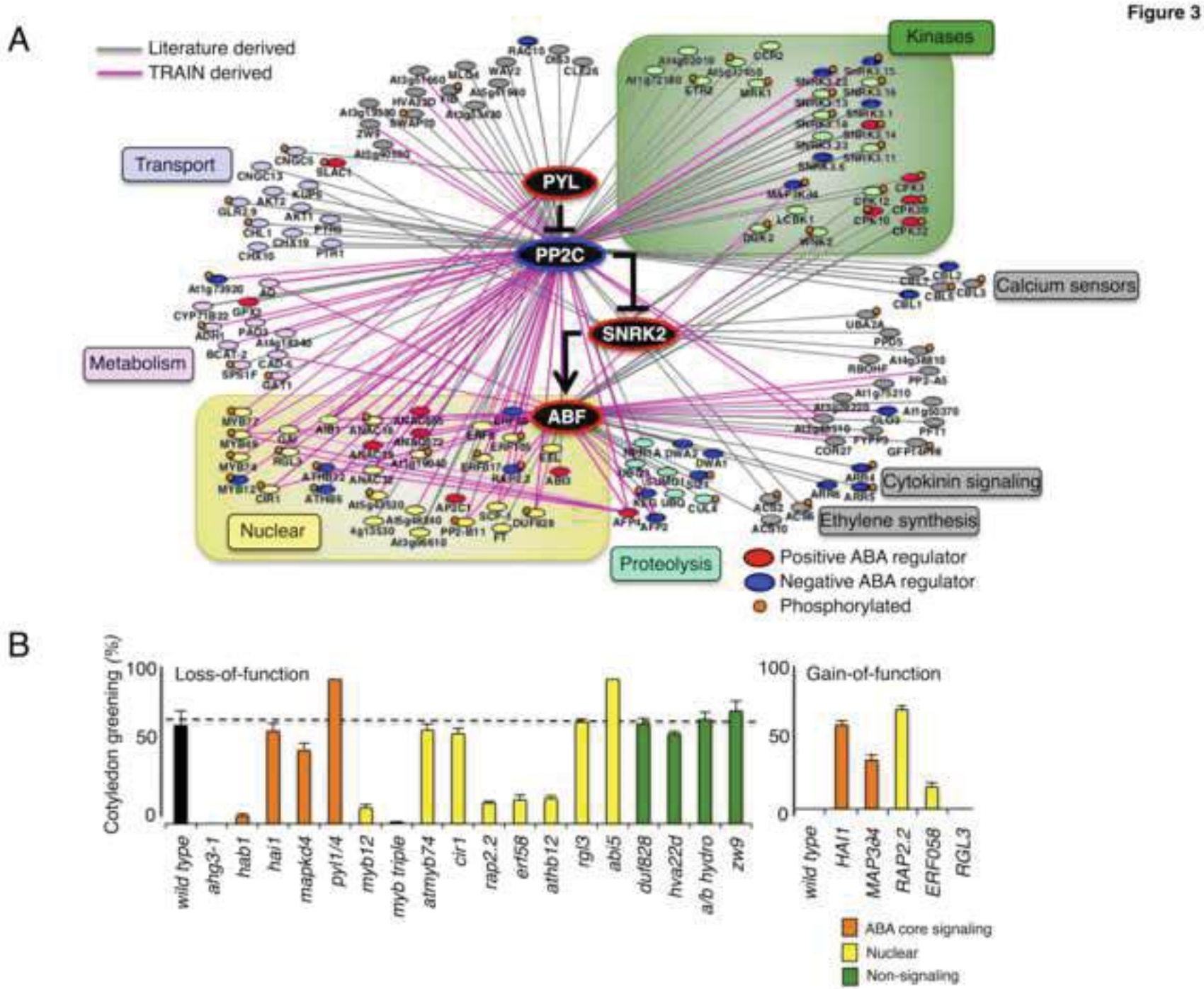

Figure 4
Click here to download high resolution image

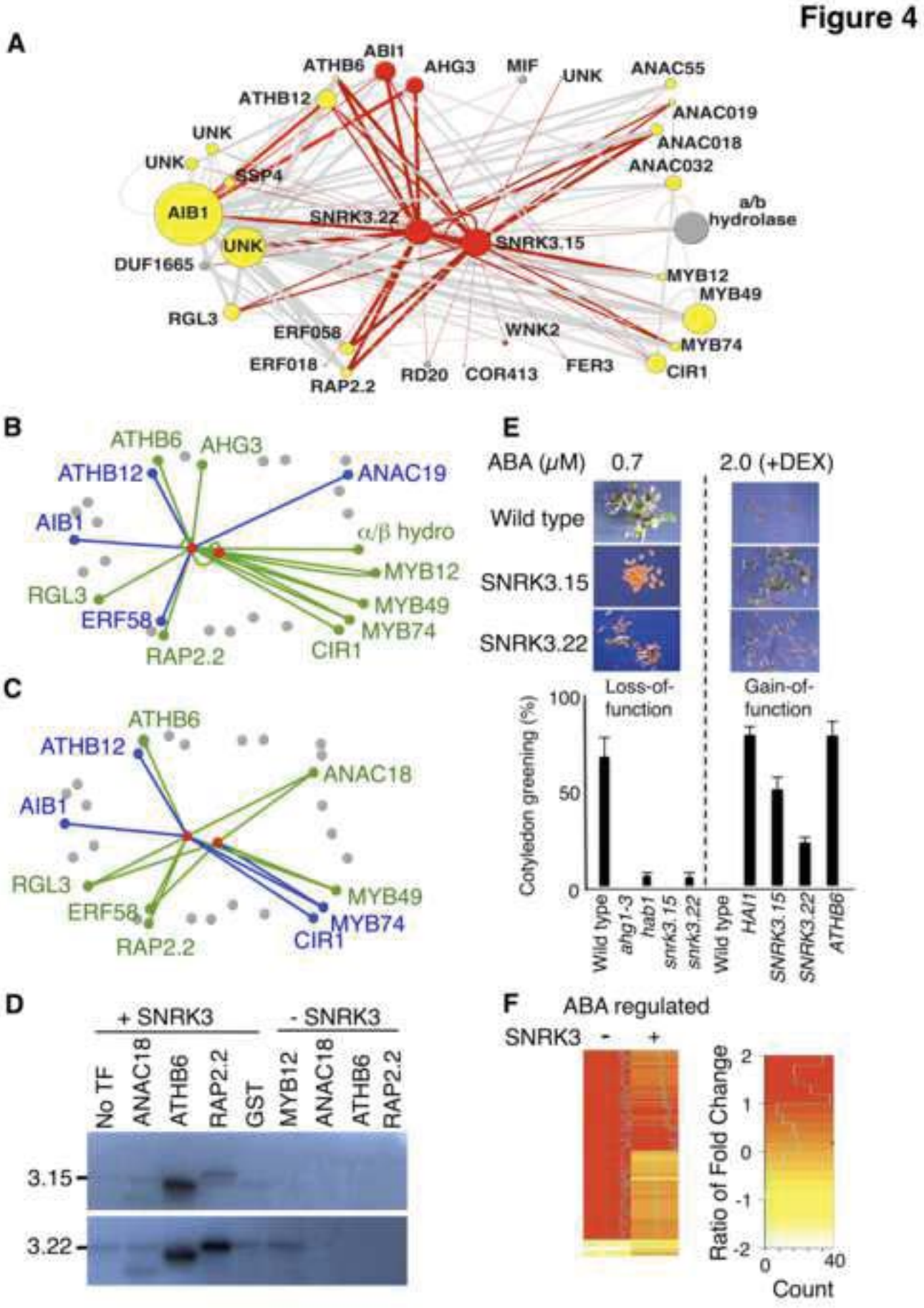

Figure 5
Click here to download high resolution image

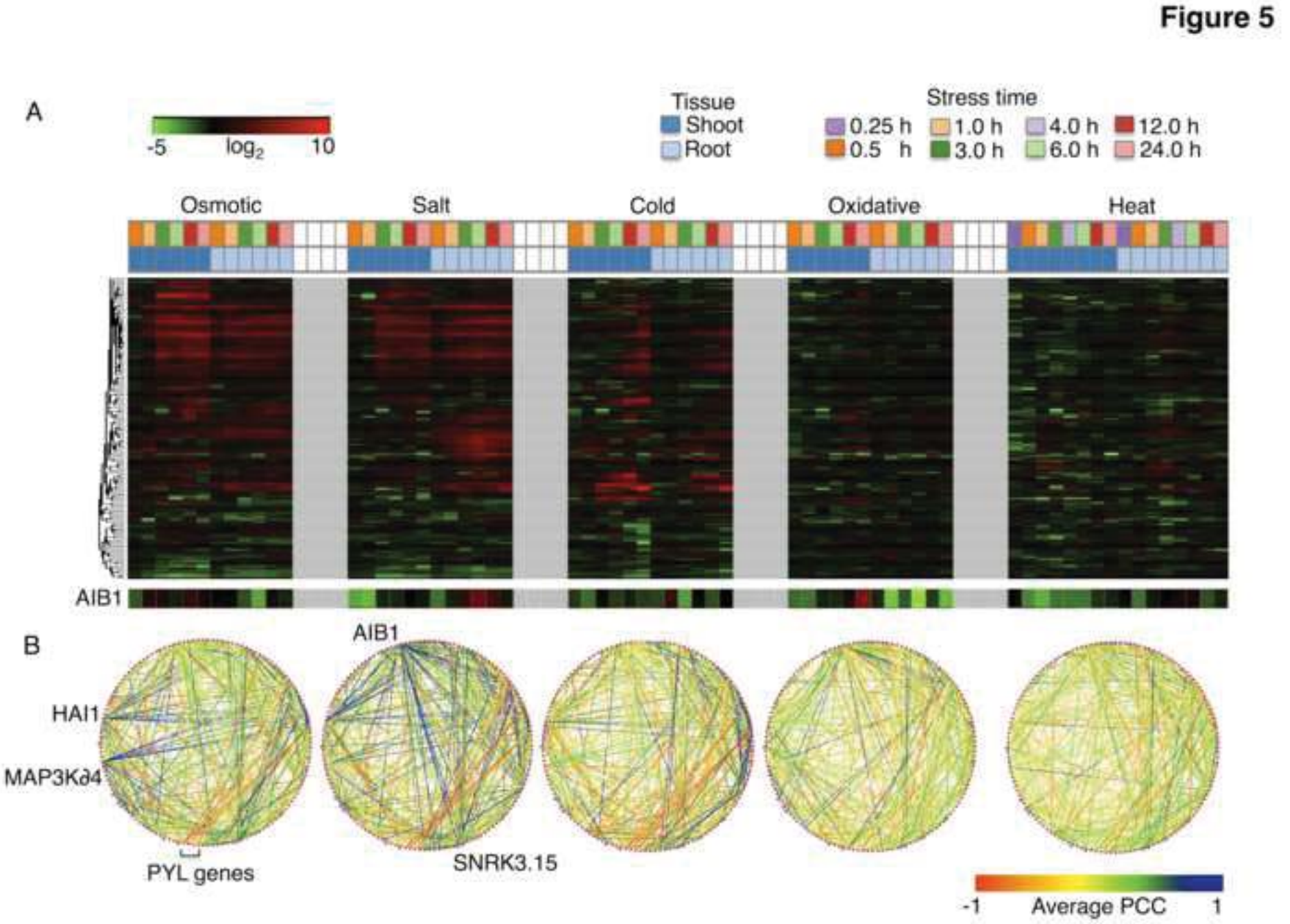

Figure 6
Click here to download high resolution image

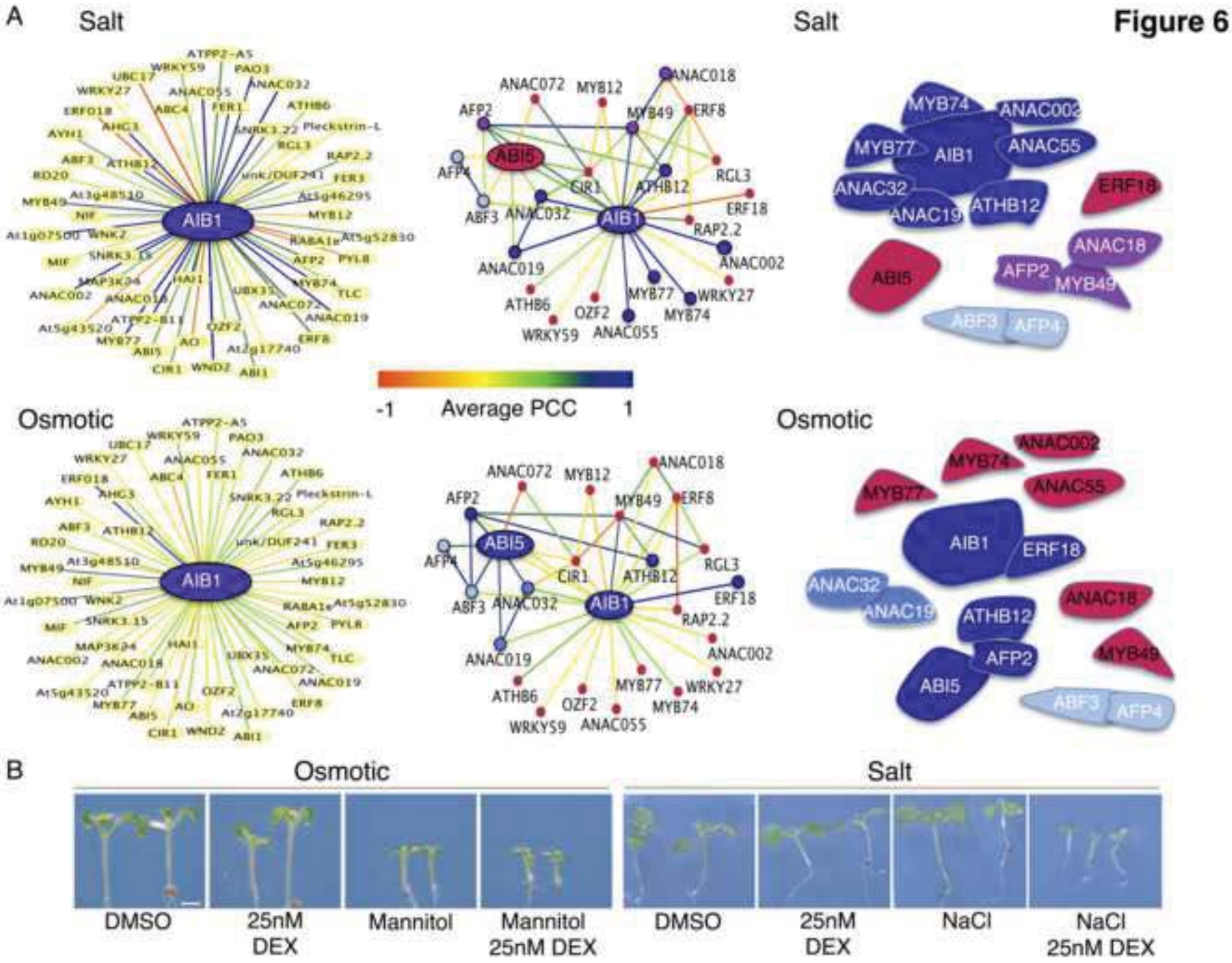

Figure 6

Supplemental Inventory

Supplemental Figure S1-S6

Figure S1. Experimental workflow for the development of the TRAIN, Related to Supplemental Experimental Procedures and Figure 1

Protein-protein interactions (PPIs) for the TRAIN were carried out using this method. The data generated can be found in Figure 1 and subsequent Figures.

Figure S2. Yeast-2-Hybrid (Y2H) interactions of known core ABA signaling genes present in the TRAIN, Related to Figure 3

Figure S3. Bimolecular Fluorescence Complementation (BiFC) validation of TRAIN-based interactions, Related to Figure 4B

(A-D) Bimolecular Fluorescence Complementation (BiFC) analyses of SNRK3.22 and SNRK3.15 interactors.

Figure S4. Biochemical validation of TRAIN based interactions, Related to Figure 4C and D

(A) Two dimensional gel electrophoresis images of TFs in the presence or absence of SNRK3.15 or SNRK3.22. The data generated contributed to Figure 4C. (B) Phosphorylation assay of various SNRK3.15 or SNRK3.22 TF partners. The data generated contributed to Figure 4C and D.

Figure S5. Experimental workflow for the development of SNRK3.15 activation on ABA, Related to Figure 4F

(A) Experimental design for testing SNRK3.15 activation on ABA germination response. (B) Western blot analysis of transgenic plants containing a DEX-inducible SNRK3.15 cassette.

Figure S6. Interaction overlap between AIB1 and SNRK3.15 or SNRK3.22, Related to Figure 6

Table S1-S2

Table S1. Excel file of TRAIN related parameters, Related to Figures 1-4

Tab1: Tab descriptions; Tab2 282 gene set, Tab 3: ABA gene expression in wild type versus *aba2-2*. Tab S4: 258 ORFome genes, Tab S5: The TRAIN. Tab S6: TRAIN Network statistics, Tab S7: The eTRAIN. Tab S8: ABA core interactions. Tab S9: Literature derived phosphorylation sites.

Table S2. ABA responsive genes identified in DEX inducible SNRK3.15 lines, Related to Figure 4

Blue box, fold change in ± DEX inducible ± ABA. Light orange, fold change in wild type versus *snrk3* triple mutant ± ABA. Light green, fold change in aba2-2 versus wild type ± ABA. NT, non treated.

Supplemental Figure Legends

Supplemental Experimental Procedures

Supplemental References

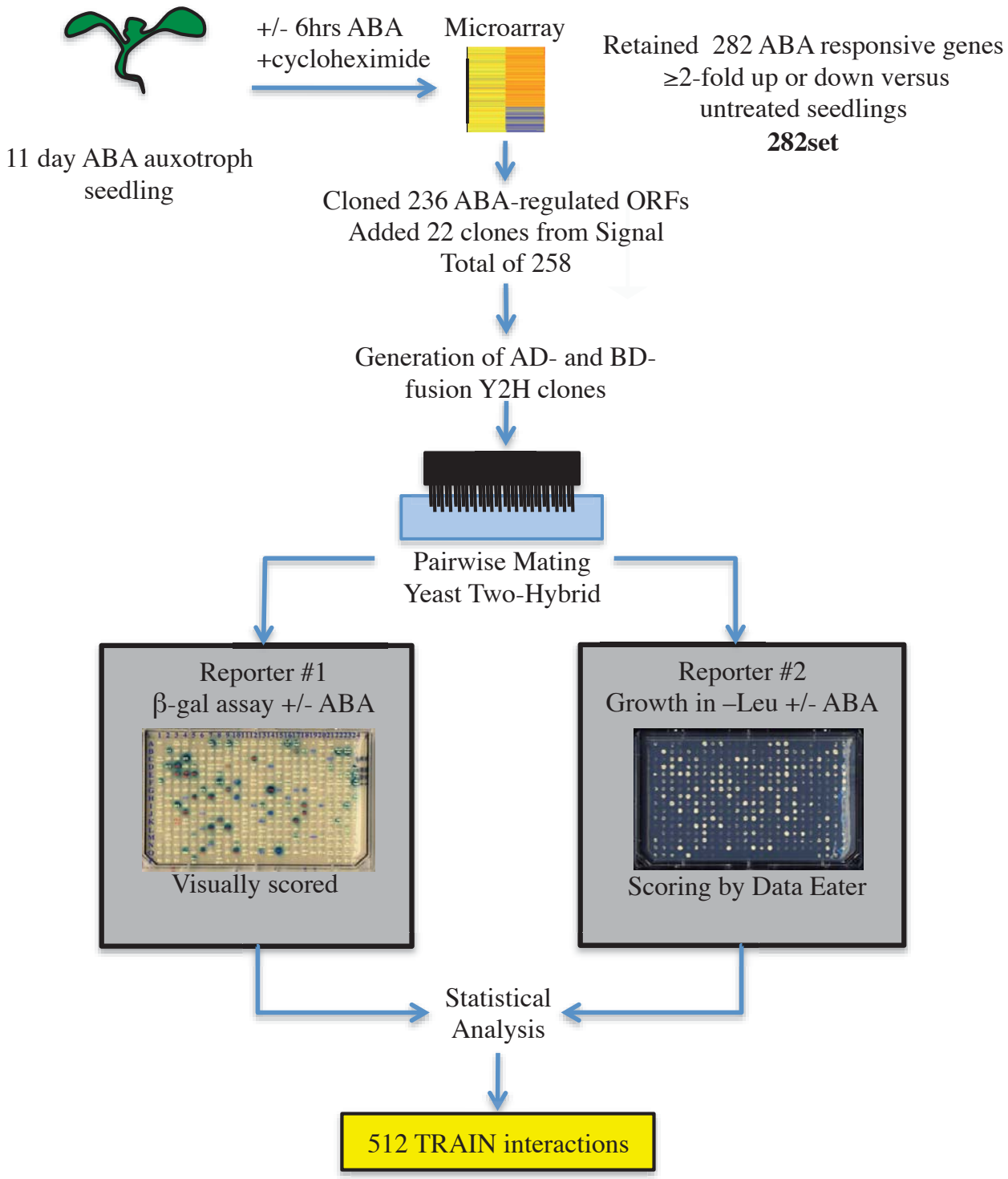

Figure S1 Lumba *et al*.

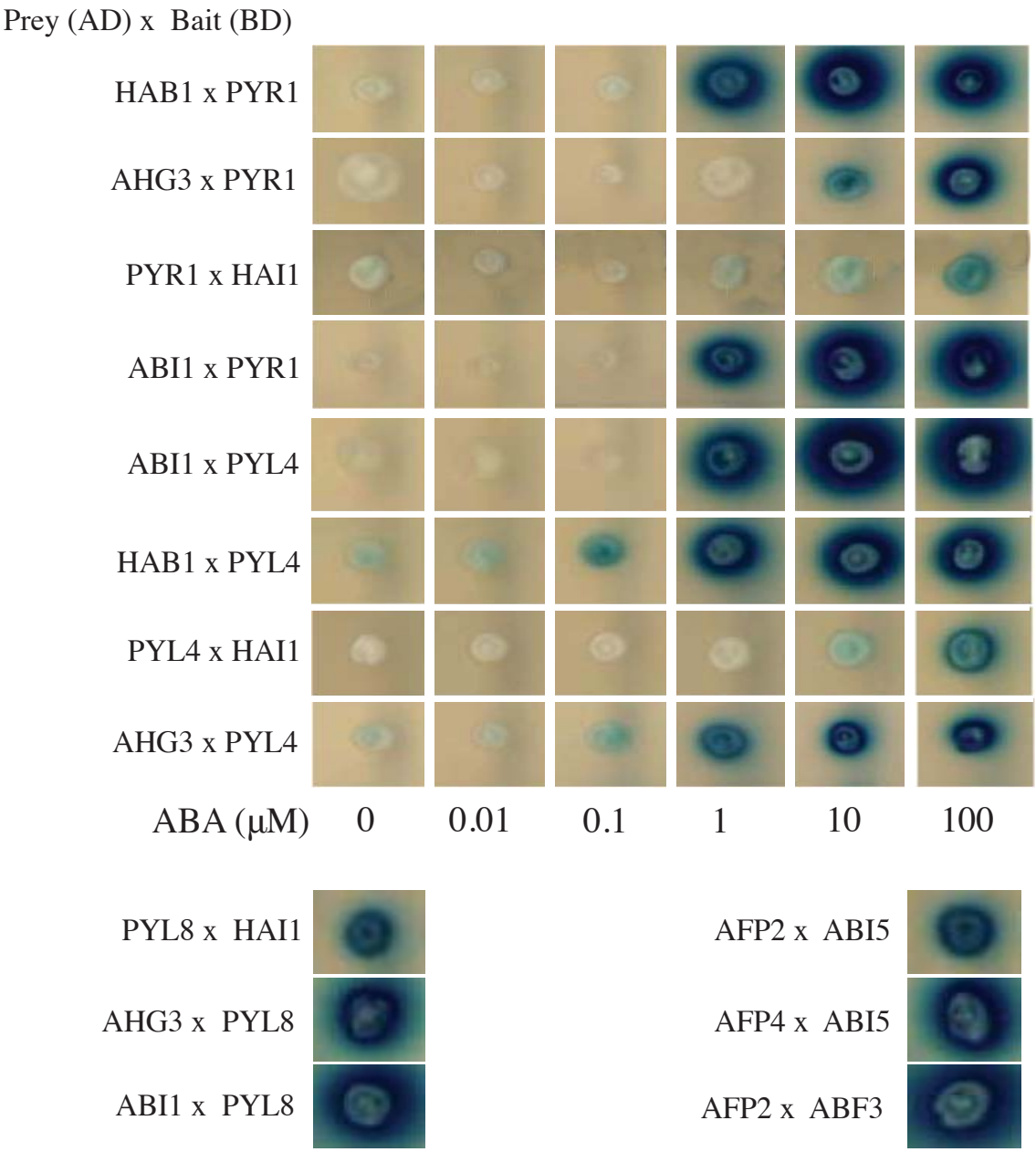

Figure S2 Lumba *et al*.

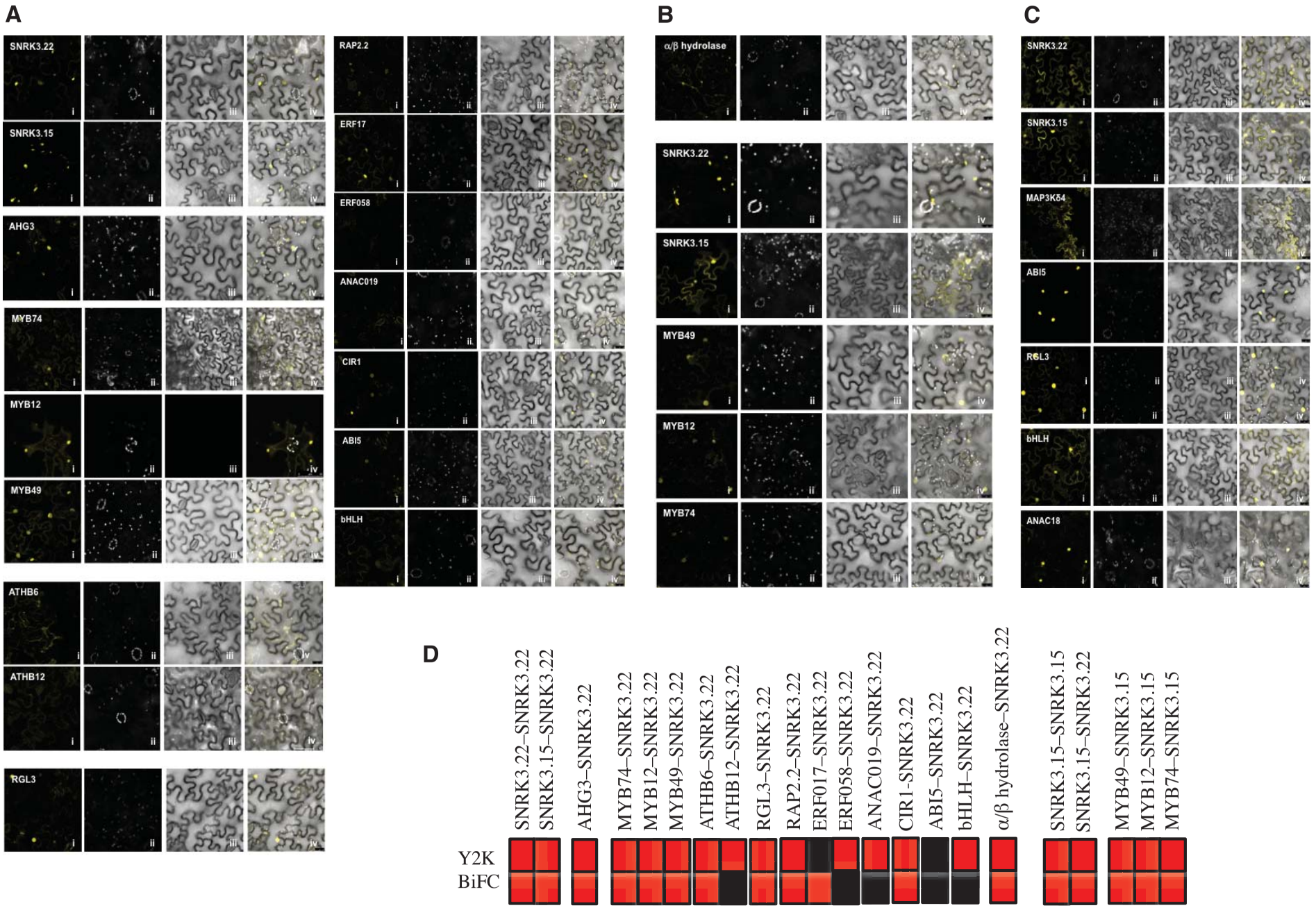

Figure S3 Lumba *et al*.

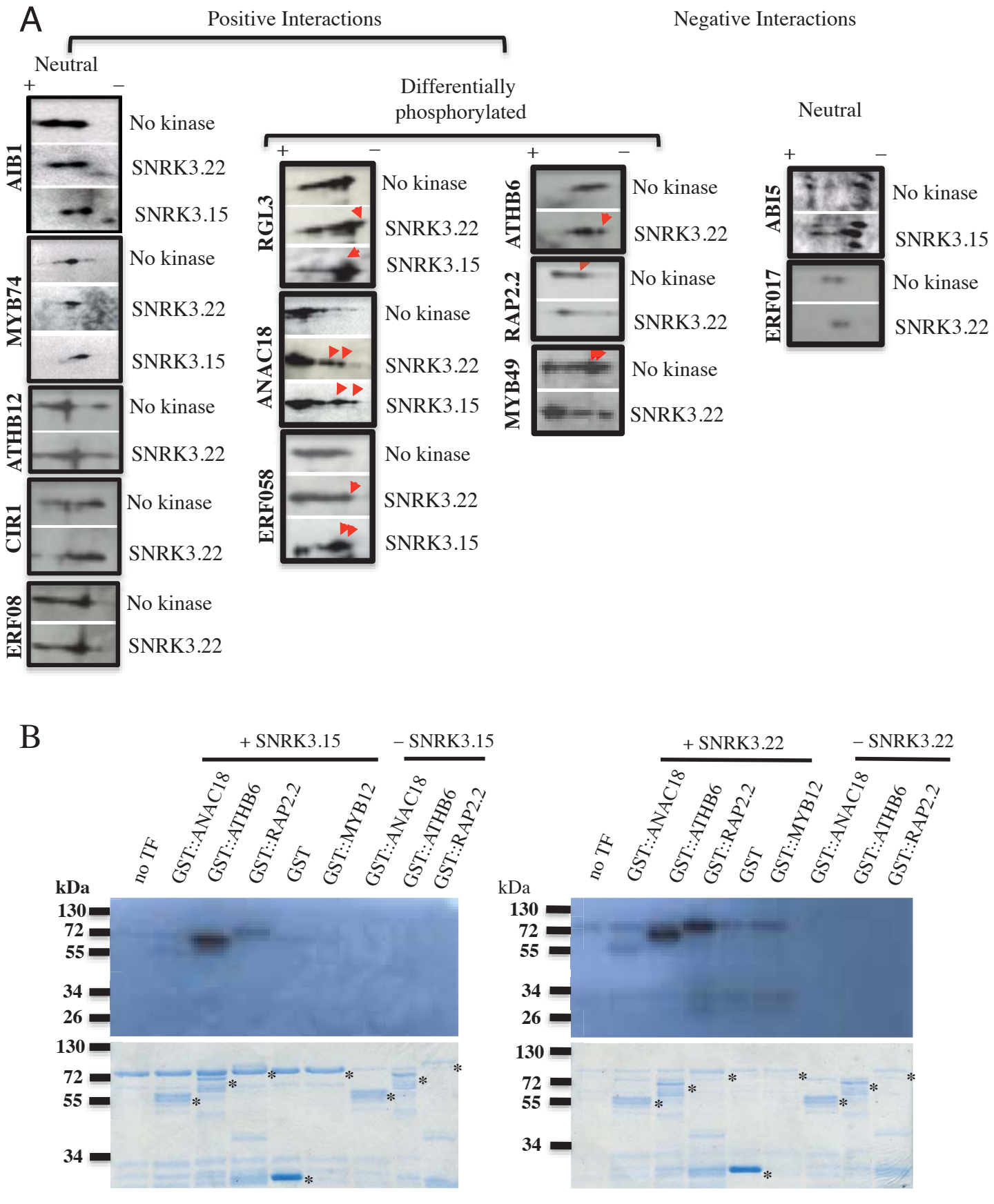

Figure S4 Lumba *et al*.

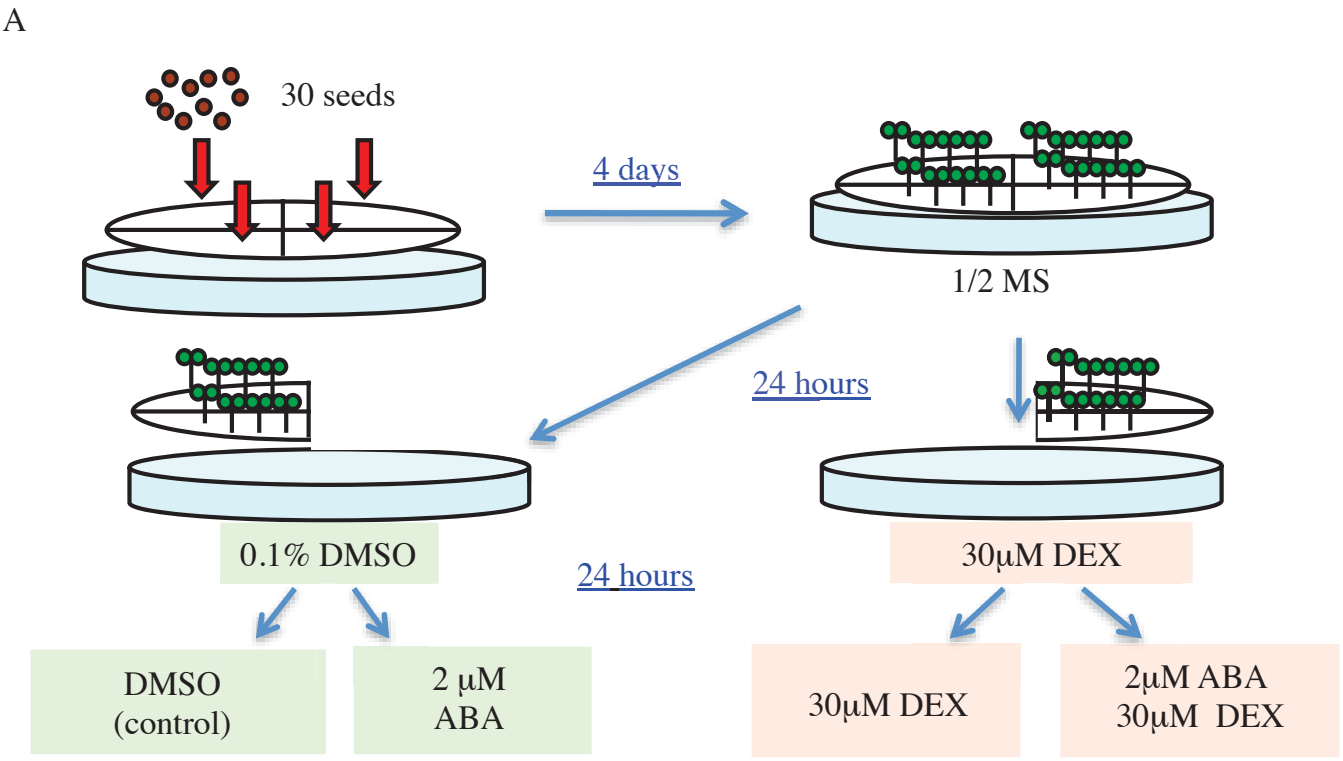

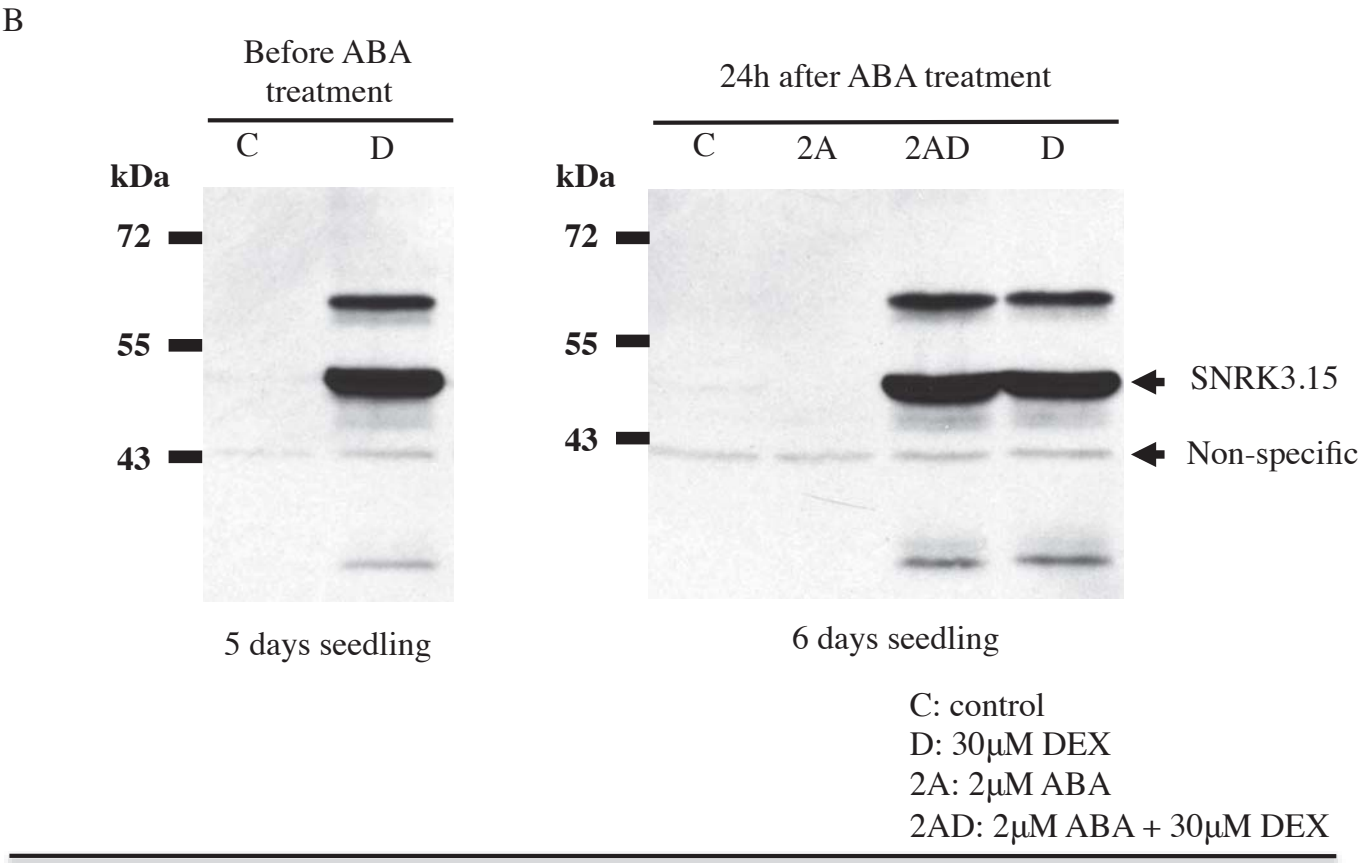

Figure S5 Lumba *et al*.

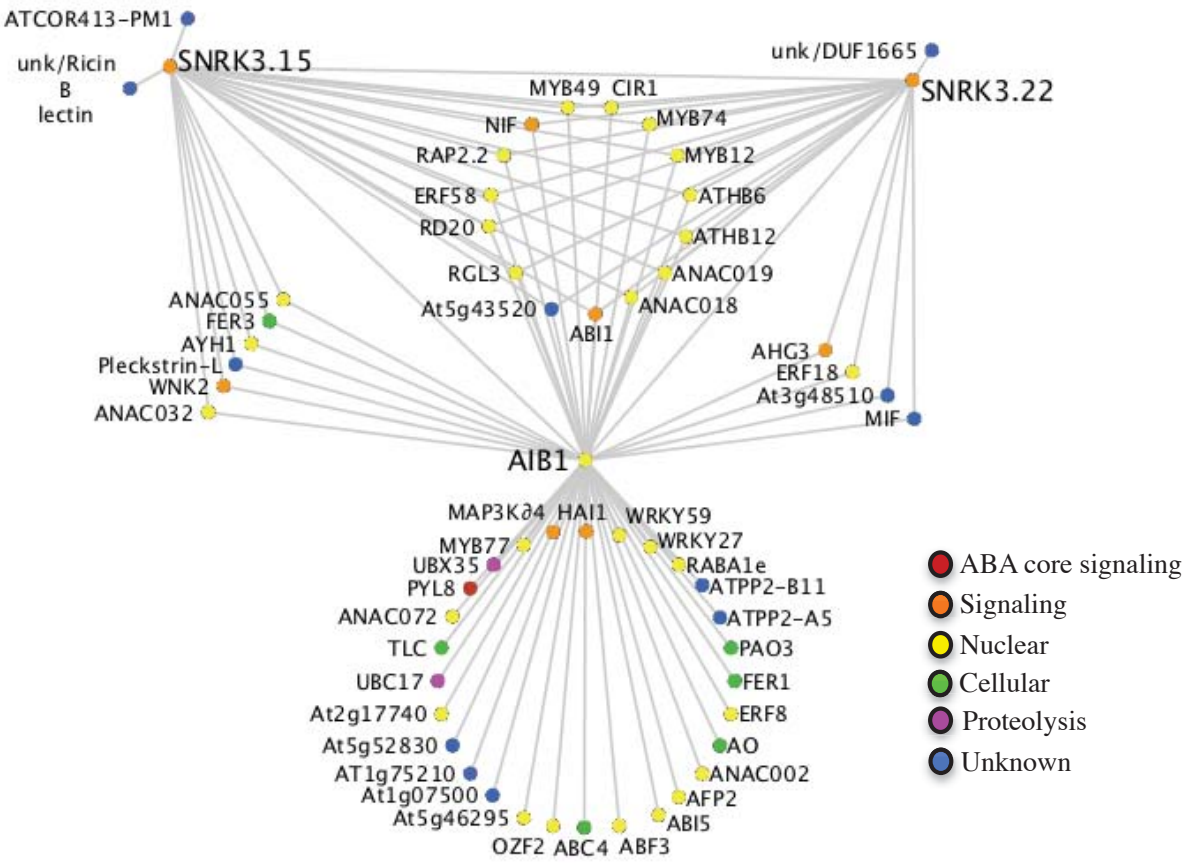

Figure S6 Lumba *et al*.

Supplemental Figure Legends

Figure S1. Experimental workflow for the development of the TRAIN, Related to Supplemental Experimental Procedures and Figure 1

AD, Activation Domain of LexA; BD, DNA-binding Domain of LexA. The yeast two-hybrid (Y2H) reporter outputs used in this study are encapsulated in gray boxes. β-gal is the reporter based on β-galactosidase activity in the presence of the X-gal substrate. A blue colony indicates the presence of an interaction. – Leu represents the reporter assay for interactions based on colony growth in the absence of leucine in the medium.

Figure S2. Yeast-2-Hybrid (Y2H) interactions of known core ABA signaling genes present in the TRAIN, Related to Figure 3

Pictures represent Y2H interactions where the first gene is the prey fused to the activation domain and the second gene is the bait fused to the DNA-binding domain. Blue color represents a positive interaction. PYR1 and PYL4 are ABA receptors that interact with PP2Cs in an ABA-dependent manner whilst PYL8 appears to interact with the PP2C partners independently of ABA. *AFP2* and *AFP4* encode *A*BI5 *B*inding *P*roteins that have been previously shown to interact with ABI5 and may be involved in ABI5 protein turnover. We also found an interaction between the bZIP TF proteins ABI5 and ABF3.

Figure S3. Bimolecular Fluorescence Complementation (BiFC) validation of TRAIN-based interactions, Related to Figure 4B

Representative pictures of BiFC analyses in leaves of *Nicotiana benthamiana* of SNRK3.22 and SNRK3.15 interactors queried against a collection of positive and negative Y2H-based interactors. The images included are: (i) YFP, (ii) autofluorescence, (iii) DIC, and (iv) merged. Several replicates were observed for each combination. (A) SNRK3.22 fused to the C-terminal portion of YFP (YFPc-SNRK3.22) in combination with interacting proteins from ABA interactome fused to the N-terminal portion of YFP. (B) SNRK3.15 fused to the C-terminal portion of YFP (YFPc-SNRK3.15) in combination with interacting proteins from ABA interactome fused to the N-terminal portion of YFP. (C) Visualization of select full-length proteins from ABA interactome fused to YFP. (D) Summary comparison of Y2H to BiFC analysis. Red color means an interaction was detected. Black denotes that no interaction was identified.

Figure S4. Biochemical validation of TRAIN based interactions, Related to Figure 4C and D

(A) Two dimensional gel electrophoresis images of TFs in the presence or absence of SNRK3.15 or SNRK3.22. TFs were detected using a HA translational fusion and were detected using a HA specific antibody. Neutral; no clear shift of a spot was detected. Differential phosphorylated; a reproducible shift in a spot was detected. In most cases the

shift is consistent with a SNRK3 dependent modification. However, in the case of RAP2.2 and MYB49, a shift was detected in the absence of the kinase but not in the presence. This suggested a yeast protein can modify the target TF but this modification does not occur in the presence of a SNRK3. Negative interactions; were the testing of negative TF controls (ABI5, ERF17) that did not show an Y2H interaction with either SNRK3. (B) Phosphorylation assay of various SNRK3.15 or SNRK3.22 TF partners. Purified GST tagged TFs were incubated with [^{32}P]- γ-ATP, in the presence (+) or absence (-) of a purified GST:SNRK3. Reactions were loaded onto 12% SDS-PAGE gels, and incorporated radiolabel was visualized by autoradiography (upper gel). As loading controls, proteins used in the kinase assays were run on SDS-PAGE gels and visualized by Coomassie blue staining (lower gel). Molecular weights (kiloDaltons) of SNRK3s and TF partner proteins. Mwt include GST fusion: SNRK3.22-GST (~ 80 kDa), SNRK3.15-GST (~ 80 kDa), ATHB6-GST (~ 65 kDa), ANAC18-GST (~ 65 kDa), RAP2.2-GST (~ 72 kDa), MYB12-GST (~ 71 kDa). See Supplemental Experimental Procedures for details.

Figure S5. Experimental workflow for the development of SNRK3.15 activation on ABA, Related to Figure 4F

(A) Experimental design for testing SNRK3.15 activation on ABA germination response. See Supplemental Experimental Procedures for details. (B) Western blot analysis of transgenic plants containing a DEX-inducible SNRK3.15 cassette. Proteins were loaded onto 12% SDS-PAGE gels, an HA::SNRK3.15 translational fusion was detected using an HA specific antibody in the absence and presence of 30μM DEX. Raw data can be found in Table S2.

Figure S6. Interaction overlap between AIB1 and SNRK3.15 or SNRK3.22, Related to Figure 6

Proteins that interact with SNRK3.15 (24/26) and SNRK3.22 (22/23) also partner with AIB1.

Table S1-S2

Table S1. Excel file of TRAIN related parameters, Related to Figures 1-4

Tab1: Tab descriptions; Tab S2: 282 gene set, Tab S3: ABA induction wild type versus aba2; Tab S4 258 ORFome genes, Tab S5: The TRAIN. Tab S6: TRAIN Network statistics; Tab S7: The eTRAIN. Tab S8: ABA core interactions. Tab S9: Literature derived phosphorylation sites.

Table S2. ABA responsive genes identified in DEX inducible SNRK3.15 lines, Related to Figure 4

Blue box, fold change in ± DEX inducible ± ABA. Light orange, fold change in wild type

versus *snrk3* triple mutant ± ABA. Light green, fold change in aba2-2 versus wild type ± ABA. NT, non treated.

Supplemental Experimental Procedures

Plant material and growth conditions. All Arabidopsis strains used in this study were of the ecotype Columbia (Col-0). Propagation of strains was done under 24 hour light in pots. All seedling-based experiments were performed at room temperature under a light fluence of 55-60 μmol m^{-2} s^{-1} for five to seven days. For sterile growth, seeds were germinated on 0.8% agar 0.5 X minimal media consisting of Murashige and Skoog mineral salts (MS) (1). Identification of loss-of-function lines was performed by ordering the appropriate SALK knockout lines from SIGnAL (http://signal.salk.edu/) and subsequently each line was verified by standard PCR analysis as suggested by SIGnAL.

For the construction of transgenic DEX inducible Arabidopsis lines the floral dip method was used to transform Arabidopsis (Col) with the various gene constructs (Bent, 2006). Twelve lines were selected from the transformed (T1) batch of seeds using resistance to the herbicide glufosinate (Basta) as the selectable marker. The number of insertions was determined based on the segregation ratio on Basta in the T2 generation. Four individual lines showing a simple Mendelian ratio of Basta resistance in the T2 generation were propagated for each transgenic line and validated to be homozygous. Only homozygous T3 seeds were used for experiments. For double mutant analysis between DEX inducible transgenic plants and the ABA hypersensitive line, *ahg3-1*, crosses were made between lines and F2 seedlings were genotyped for the *ahg3-1* mutation and particular DEX insertion. The *ahg3-1* mutation was verified using the dCAPs marker (Forward primer 5'-TCAGTGTGACGCCGTCGGATC-3'; Reverse primer 5'-AATTGCTCTAGAC ATGGCAAGAATT-3').

For germination and early seedling growth experiments, seeds were imbibed on 1/2X MS plate for 4°C for four to five days before being transferred to 24°C under continuous white light. Light intensity was 55-60 μM m^{-2} s^{-1}. For ABA hypersensitivity germination experiments, plates contained 0 or 0.7 μM ABA respectively and germination was scored after seven days at room temperature. At 0 ABA concentrations wild type seeds showed 100% germination whilst on 0.7 μM ABA, wild type seeds germination was 68 ± 5% SD. The average was subtracted from mutant seed germination rates to normalized values across both loss- and gain-of-function experiments. For ABA insensitive experiments again seeds were plated 1/2X MS plate for 4°C for four days before being

transferred to 24°C under continuous white light condition. DEX induction was performed by plating seeds on either 0.1% DMSO or 50 nM DEX. Germination of wild type on 2μM ABA was 0. For salt and mannitol stress experiments seeds were sterilized, imbibed at 4^0C for 4 days on 0.5X MS and then germinated and grown for 7 days at room temperature 100-150 μEinstein. Mannitol concentrations were tested from 1-5% and NaCl from 25 to 300 mM.

Construction of the Transcriptionally Regulated ABA Interactome Network (TRAIN)

Cloning of Full Length ABA-regulated ORFs from the 282set. The general outline was published in Park *et al*., 2009. A more detailed description is provided below. Using the 282set as a reference for ABA-regulated transcripts, total RNA was isolated from 11-day old Arabidopsis seedlings grown in the presence of 1 μM ABA and 10 μM cycloheximide using Trizol reagent (Invitrogen, Carlsbad, CA). To generate the 282set, RNA was processed and hybridized on a GeneChip Arabidopsis ATH1 genome array (representing ~22,800 genes) according to standard Affymetrix (Santa Clara, CA) protocols. Gene expression data are stored in the ArrayExpress database (http://www.ebi.ac.uk/arrayexpress, E-MEXP-3404). In addition, first-strand cDNA was synthesized using SuperScript II Reverse Transcriptase (Invitrogen) from the RNA extracted. From this cDNA sample, 224 full-length cDNAs were amplified by $Vent_R$ DNA polymerase (NEB, Ipswich, MA) whilst truncated versions or individual domains were amplified for 12 genes. The PCR products were cloned into Gateway-compatible pENTR D-TOPO vector (Invitrogen, Carlsbad, CA). To supplement the collection, 22 full-length sequence-verified cDNA clones in Gateway-compatible vectors were obtained from SIGnAL (Salk Institute, La Jolla, CA) for a final total of 258 ORFs, hereby referred to as the "ABA ORFeome". See Table S1. This represents 91% of the 282set. The ORFs were subcloned into yeast vectors, pJG4-5 and pEG202 using LR Clonase II enzyme mix, to generate fusions with the B42 activation (AD-X) and DNA-binding domains (DB-Y) of LexA, respectively. Yeast two-hybrid assays were performed using the DuplexA system (Clontech; http://www.biogen.org.ua/pdf/Origene.pdf). The pJG4-5 constructs (AD-X) were

transformed into yeast strain, EGY48 (*MATα)* and pEG202 constructs (DB-Y) were transformed into a *MATa* yeast strain, RFY206 carrying the *lacZ* reporter plasmid pSH18-34. The Frozen-EZ Yeast Transformation II Kit (Zymo Research; http://www.zymoresearch.com) was used to generate competent yeast cells and perform small-scale lithium acetate transformations. Growth and selection of yeast clones were performed as outlined in the Clontech Yeast Protocols Handbook. Yeast clones of each mating type were arrayed manually in a 384-sample format by an E-clip style 384-pin replicator tool and a registration tool, colony copier from V&P Scientific Inc. (http://www.vp-scientific.com/floating_e-clip_replicators.htm)

Yeast Two-hybrid (Y2H) Screening. To perform pair wise matings, individual AD-X strains were grown at 30 °C overnight in 3 mL liquid culture (query strain). The culture was spread on a selective plate to generate a lawn after two days of growth. The ORFeome library consisting of all DB-Y strains was replicated in 384-sample format and grown for two days at 30 °C. Matings were done on a rich yeast media (YPD) onto which the DB-Y library was pinned. A 384-replicator was used to overlay one query strain onto the library for pair wise matings, which were done at 30 °C overnight. Two independent matings were performed for each AD-X strain. To ensure that diploids were obtained, the colonies were transferred twice using the 384-pin tool and grown for 2 days at 30 °C on selective media plates. Each set of diploids was pinned to two types of reporter plates, one screening for β-galactosidase activity on X-gal plates and the other for growth in the absence of leucine. Each reporter was also assayed in the presence of 100 μM ABA. Thus, pair wise assays were performed a total of eight times, four to test β-galactosidase activity on X-gal plates and four to screen for growth in the absence of leucine. Reporter plates were scanned on a Canon 8600 scanner after two and four days of growth at 30 °C. Construction of the TRAIN is summarized on Figure S1.

Data extraction for X-gal: Because the data from X-gal did not show regularly shaped spots, it could not be analyzed automatically as with the minus Leucine data described above. Therefore, each spot was scored manually using a discrete scale of Dark, Light,

Very Light, or no blue staining. Autoactivators were defined as interactions that appeared repeatedly in many experiments. For scoring of β-galactosidase activity, a visual determination was used where colonies were scored negative (white), weak interaction (very light blue), medium interaction (light blue) or strong interaction (dark blue). An interaction was deemed positive if it was observed in all four X-gal reporter plates. Autoactivators were defined as interactions that appeared repeatedly in many experiments per batch and were eliminated from the study.

Data extraction for minus Leucine: For scoring of growth on leucine, an application was developed to automatically quantify colony size, which will hereby referred to as **DataEater**. Each image contained 4 plates, from which the orientation of the spots was slightly different. To automatically identify the grid position, **DataEater** performed a local search of possible grid orientations. The pixel intensity of cell colonies was used for this purpose, since it was higher than the plate background. Color images were converted into intensity values using the standard grayscale conversion: I = 0.3R2.2 + 0.59G2.2 + 0.11B2.2. The search for the 16x24 spot grid was performed by maximizing the mean intensity difference between pixels from the predicted spots and their surrounding area. The proportion of the spot size and their spacing was provided, so only four parameters were to be recovered per plate (these correspond to the centre of the grid, a scaling parameter and a rotation parameter). The simulated annealing search often led to a local maximum where the found grid was often missing an edge row or column, usually because either all their colony sizes are small or some lighting artifacts affected the image. Each grid was therefore manually adjusted, by shifting current grid rows or columns to capture the missing ones. If needed, the manually adjusted grid could be used as starting guess for a new search procedure. Visual inspection of each grid ensured that there were no misplaced grids before data extraction.

In order to extract measurements of individual colony's sizes, **DataEater** used their pixel average intensities. The background pixels are modeled as a Gaussian distribution, while the colony pixels are modeled with a uniform distribution, whose minimum is the mean for the background distribution and maximum matches the highest representable pixel intensity for the image. The maximum likelihood parameters are recovered for each

plate (using Expectation-Maximization, EM) modeling the whole rectangular area containing the grid of spot. Finally, the posterior probability of each pixel having been part of the colony was computed. The colony intensity was measured using the mean intensity of the pixels weighted by their posterior probability that there were part of the colony.

Spots at the edges of the plates were then removed from further analysis, as they tended to grow larger due to medium availability. Experiments were done in quadruplicate, so that each spot's intensity was measured 4 times. These were compared to 11 negative control (empty vector) spots (44 total measurements) by computing a two-sample t-statistic:

$$t_{ij} = \frac{\mu_{ij} - \mu_{EVi}}{\sqrt{\frac{(n_{ij}-1) * {\sigma_{ij}}^2 + (n_{EVi}-1) * {\sigma_{EVi}}^2}{n_{ij} + n_{EVi} - 2}}}$$

where t_{ij} is the statistic for the j^{th} spot in the i^{th} experiment, and n_{ij} (n_{EVi}) is the number of replicates, σ_{ij} (σ_{EVi}) is the standard deviation and μ_{ij} (μ_{EVi}) is the mean of the measurements for that spot (empty vector control spots). Autoactivators (defined as interactions that had t-statistics>2 in >50% of experiments) were removed from further analysis. **DataEater** automatically generates an Excel file, containing calculations of colony sizes and t-statistics for each image.

Integration of X-gal and minus Leucine data: We sought to combine both reporters and available replicates to obtain the most confident set of interactions. To do so, we devised a simple generative model, where the true status of an interaction was considered to be a "hidden" binary variable that indicates whether a particular bait interacts with a particular prey. The X-gal and Leucine data were considered to be conditionally independent given the state of this hidden variable, and modeled using multinomial and Gaussian distributions respectively. The log likelihood of this model is given by

$$logL = \sum_i \log \sum_{Z\in\{0,1\}} p(Z)p(X_i, t_i|Z_i) = \sum_i \log \sum_{Z\in\{0,1\}} p(Z) \prod_{j\in Xgal} p\left(X_{ij}\middle|f, Z_i\right) \prod_{j\in Leu} p(t_{ij}|\mu, \sigma, Z_i)$$

Where X_{ij}, t_{ij} are the values of the for j^{th} datapoint of X-gal data and leucine data for the

i^{th} interaction, respectively; Z_i is the hidden variable for the i^{th} interaction, f and μ,σ are the parameters of the multinomial, and Gaussian, respectively for the two possible values of Z. Because the X-gal data is modeled as multinomial, X_{ij} is an indicator variable whose k^{th} component represents the k^{th} possible observation among the 4 possibilities: no staining, very light staining, light staining, dark staining. The prior probability of observing an interaction p(Z) was assumed to be 1%, and the other parameters were estimated using EM. The parameter updates are

$$\mu_Z = \frac{\sum_{ij} p(Z_i|t_i,X_i)t_{ij}}{\sum_{ij} p(Z_i|t,X_i)},\ \sigma_Z = \sqrt{\frac{\sum_{ij} p(Z_i|t_i,X_i)t_i^2}{\sum_{ij} p(Z_i|t,X_i)} - \left[\frac{\sum_{ij} p(Z_i|t_i,X_i)t_{ij}}{\sum_{ij} p(Z_i|t,X_i)}\right]^2} \text{ and } f_{Zk} = \frac{\sum_{ij} p(Z_i|t_i,X_i)^{X_{ijk}}}{\sum_{ij} p(Z_i|t,X_i)},$$

where the posterior, $p(Z_i\ |t_i,X_i)$, is computed using the parameter estimate from the previous iteration using Bayes' theorem:

$$p(Z_i|t_i,X_i) = \frac{p(Z)p(X_i,t_i|Z_i)}{\sum_{Z\in\{0,1\}} p(Z)p(X_i,t_i|Z_i)}$$

Each interaction was then assigned a likelihood ratio, which measured the evidence supporting each possible interaction that incorporated all available replicates and both types of reporter data. The likelihood ratio cutoff of 4.6 was used to define the 364 most confident interactions, as it represents the maximum *a posteriori* probability (MAP) classification threshold. The entire set of interactions above this cutoff is available in Table S1.

$$LR_i = \frac{p(X_i,t_i|Z_i=1)}{p(X_i,t_i|Z_i=0)} = \frac{\prod_{j\in Xgal} p(X_{ij}|f,Z_i=1)\prod_{j\in Leu} p(t_{ij}|\mu,\sigma,Z_i=1)}{\prod_{j\in Xgal} p(X_{ij}|f,Z_i=0)\prod_{j\in Leu} p(t_{ij}|\mu,\sigma,Z_i=0)} > \frac{p(Z=0)}{p(Z=1)}$$

For example, interactions for which only Leucine or only X-gal data were available (e.g., they were autoactivators in one of the reporters) could still be included by considering the strength of the evidence based on the data that was available. The most strongly supported interaction observed (log-likelihood ratio = 22.49) was between At5g59220 and At3g11410, which was observed in three replicate experiments in minus leucine (t-statistic: 6.296184757 3.842244808 3.411289581) and three replicate experiments using X-gal (dark staining observed 3 times).

High Resolution retesting of the focused SNRK3 module protein-protein interactions set: To validate the SNRK3 module first all clones of this module were sequenced and those containing errors were eliminated from the interactome. Furthermore, SNRK3 modular proteins were also ordered from sequenced full length cDNA collection at SIGnAL (http://signal.salk.edu/) SNRK3 module clones obtained from SIGnAL were also tested for protein-protein interactions by yeast two-hybrid using β-galactosidase activity and growth in the absence of leucine. SIGnAL clones were also queried against our ORFeome set as well as the SIGnAL set, which consisted of 180 ABA-regulated ORFs from the 282set. Thus, a total of 16 independent Y2H assays were performed on each protein pair within the SNRK3 module. The results of these assays were analyzed as described above.

Microarray analysis of DEX inducible *SNRK3.15* lines

Sterile seeds were plated on filter paper placed on a 1/2X MS plate and seeds were stratified for four days at 4°C. Seeds were transferred to room temperature under continuous white light for 4 days after which time, the seedlings were moved either to a 0.1% DMSO (C) or a 30μM DEX (D) plate for 24 hours. After this 24 hour incubation, seeds were transferred to 0.1% DMSO or 2μM ABA without 30μM DEX (2A) or with 30μM DEX (2AD) for 24 hours. RNA was analyzed by hybridization on a GeneChip *Arabidopsis* ATH1 genome array (representing ~22,800 genes) according to standard Affymetrix (Santa Clara, CA) protocols.

To verify good inducible SNRK3.15 protein production in transgenic lines, Western blots were performed using the HA tag on the SNRK3 fusion. The first antibody was anti-HA from rabbit (Invitrogen Life Sciences) and the second antibody was Goat rabbit IgG (H+L) HRP conjugated (MILLIPORE), which were diluted 1:1000 and 1:8000, respectively. SuperSignal West Pico Chemiluminescent Substrate (Thermo Fisher Scientific) was used for detection of the signal. The blocking agent used was 5% skim milk. Expression of SNRK3.15 under various conditions is shown in Figure S5B.

RNA was extracted from 100 mg of T4 seedlings using Trizol-based protocol (Invitrogen, Carlsbad, CA). RNA was processed and hybridization on a GeneChip

Arabidopsis ATH1 genome array (representing ~22,800 genes) according to standard Affymetrix (Santa Clara, CA) protocols. Triplicate arrays were performed for all four-array condition sets (DMSO (C), 2μM ABA (2A), 2μM ABA 30 μM DEX (2AD), 30 μM DEX (D) and experimental filtering was performed for the presence, absence or marginal reads for all 12 gene-chips. After this filtering 8410 genes were retained as either present or marginal for further analysis. After this filtering 8410 genes were retained as either present or marginal for further analysis. Hierarchical clustering of the gene sets was performed using Pearson correlation for distance matrix and the Average linkage in amap package. Heatmap using heatmap.2 program in gplots package in Bionconductor.[4] Gene expression data were obtained from the ArrayExpress database (http://www.ebi.ac.uk/arrayexpress, E-MEXP-3397)

Protein Purification and Kinase Assays

All clones for protein purification were cloned using Gateway technology into the pDEST15 (Invitrogen) vector, which creates an N-terminal translational fusion to GST. Proteins were expressed in BL21-Codon Plus cells (Stratagene). Cells were grown overnight at 37 °C, diluted 100-fold in 1 liter of LB media with antibiotics and grown to a density of 0.6 OD_{600}. 1mM isopropyl-b-D-thiogalactopyranoside (IPTG) was then added and cultures were grown overnight at 18 °C. Cell pellets were resuspended in lysis buffer (30 ml of 50 mM Hepes pH 8, 500 mM NaCl, 1% Triton X-100, 5 mM DTT and bacterial protease inhibitors [Sigma]), lysed using an Avestin Emulsiflex-C5 (Avestin; http://www.avestin .com) and centrifuged for 30 min at 14,000 rpm in a Beckman JA-20 rotor (Beckman Coulter). Supernatant was loaded onto a 1 ml Glutathione Sepharose 4B resin (GE Healthcare) hand poured column pre-equilibrated with lysis buffer and incubated at 4 °C for 1 hr with gentle rocking. Flow-through was discarded and resin was washed with 10 ml of lysis buffer followed by 10 ml of wash buffer (30 ml of 50 mM Hepes pH 8, 100 mM NaCl, 1% Triton X-100) and then 20 ml of elution buffer (30 ml of 50 mM Hepes pH 8, 100 mM NaCl). Protein was eluted with 10 ml of elution buffer containing 3mg/ml glutathione collected in 1 ml fractions. Identity of the purified proteins was confirmed by mass spectrometry.

Kinase reactions were conducted in 20 uL of kinase buffer (10 mM $MgCl_2$, 10 mM $MnCl_2$, 20 mM Tris pH 7.5, 10 μM ATP) with 1μCi [γ^{32}P]ATP for 15 minutes at room temperature and terminated by adding 2.2 μL of Laemmli buffer. Reactions were loaded onto 12% SDS-PAGE gels, and incorporated radiolabel was visualized by autoradiography. Typical kinase reactions contained 200ng of purified kinase and appropriate substrates. As loading controls proteins used in the kinase assays were run on SDS-PAGE gels and visualized by Coomassie blue staining.

Gene Expression Analysis

Gene expression data was generated from the AtGenExpress global stress expression data set. The data were downloaded from the BAR http://dx.doi.org/10.1111/j.1365-313X.2005.02437.x) or from GEO (Toufighi, K. et *al* 2005). The expression platform used in all cases was the ATH1 GeneChip from Affymetrix. The data sets and comparisons were as follows: *aba2-2* seedlings (1 comparison: 6 hr with 1 μM ABA vs. mock-treated plant; this publication – data available from the BAR at http://bar.utoronto.ca/affydb/cgi-bin/affy_db_proj_viewer.cgi?proj=26&view=general). Wild type Col-0 seedlings (3 comparisons: 30 min, 1 hr or 3 hr 10 μM ABA vs. appropriate control, were based on RIKEN generated experiments http://dx.doi.org/10.1111/j.1365-313X.2008.03510.x, Goda et al., 2008). The Affymetrix CEL files for these experiments were loaded into BioConductor (http://dx.doi.org/10.1186/gb-2004-5-10-r80) and were normalized with the GCOS/MAS5 algorithm with the TGT value set to 500 (Gentleman et al, 2004). Probe sets were filtered to such that any probe sets with a call of "absent" in any sample were eliminated, i.e. probe sets had to be called "present" or "marginal" in all samples. Because some of the data sets only contained duplicated samples thereby precluding a more rigorous statistical analysis, for each probe set we computed the ratio of the average GCOS/MAS5 expression signal in the treated sample replicates to the average GCOS/MAS5 expression signal in the control sample replicates. Two-fold or more "up" or "down"-regulated gene lists were generated for each of the comparisons above. Heatmaps of osmotic stress related gene expression were generated using GENE-E (http://www.broadinstitute.org/cancer/software/GENE-E/index.html). Hierarchical

clustering was performed on rows using a row distance metric of one minus the Pearson correlation.

Supplemental References

Bent, A. (2006). *Arabidopsis thaliana* floral dip transformation method. Methods Mol. Biol. *343*, 87–103.

Goda, H. et al. (2008). The AtGenExpress hormone and chemical treatment data set: experimental design, data evaluation, model data analysis and data access. Plant J. *55*, 526-542.

Gentleman, R.C. et al. (2004). Bioconductor: open software development for computational biology and bioinformatics. Genome Biol. *5*, R80

Toufighi, K. *et al*. (2005). The Botany Array Resource: e-Northerns, Expression Angling, and promoter analyses. Plant J *43*, 153-163.